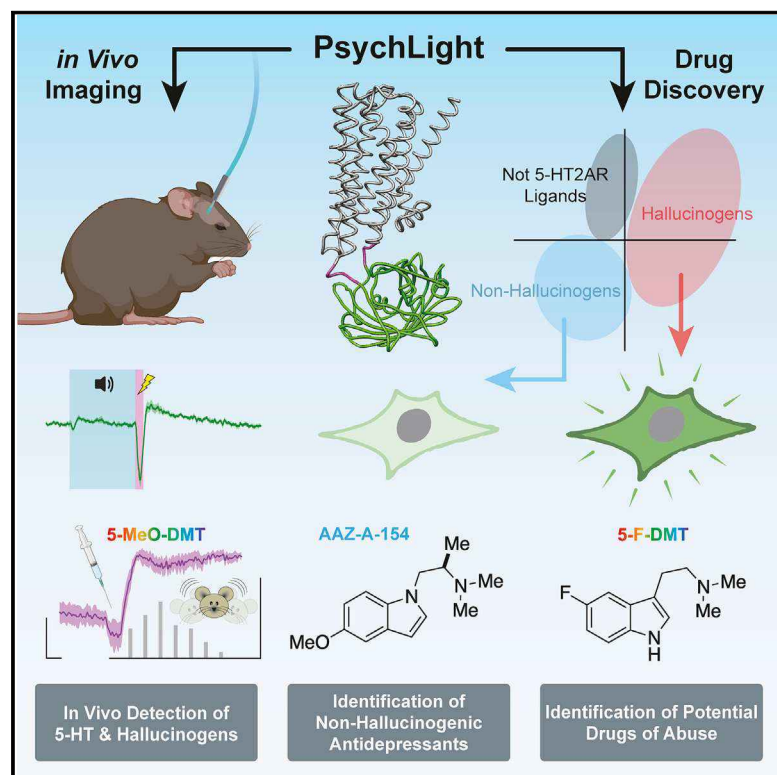# Psychedelic-inspired drug discovery using an engineered biosensor

Graphical abstract

Authors

Chunyang Dong, Calvin Ly,
Lee E. Dunlap, ..., William C. Wetsel,
David E. Olson, Lin Tian

Correspondence

deolson@ucdavis.edu (D.E.O.),
lintian@ucdavis.edu (L.T.)

In brief

Engineered biosensor based on 5-HT2AR structure enables the identification of designer drugs of abuse and the development of non-hallucinogenic therapies

Highlights

- Engineered psychLight—a genetically encoded 5-HT sensor based on the 5-HT2AR

- PsychLight can measure 5-HT dynamics in behaving mice

- A psychLight-based cellular imaging platform predicts hallucinogenic potential

- Identified a non-hallucinogenic psychedelic analog with antidepressant properties

CellPress

Cell

Psychedelic-inspired drug discovery using an engineered biosensor

Chunyang Dong,[1,6,8] Calvin Ly,[2,8] Lee E. Dunlap,[2,8] Maxemiliano V. Vargas,[3] Junqing Sun,[6] In-Wook Hwang,[4] Arya Azinfar,[2] Won Chan Oh,[4] William C. Wetsel,[5] David E. Olson,[2,6,7,*] and Lin Tian[6,7,9,*]

[1]Graduate Program in Biochemistry, Molecular, Cellular, Developmental Biology, University of California, Davis, Davis, CA 95616, USA
[2]Department of Chemistry, University of California, Davis, One Shields Avenue, Davis, CA 95616, USA
[3]Neuroscience Graduate Program, University of California, Davis, Davis, CA 95618, USA
[4]Department of Pharmacology, University of Colorado School of Medicine, Anschutz Medical Campus, Aurora, CO 80045, USA
[5]Departments of Psychiatry and Behavioral Sciences, Cell Biology, and Neurobiology, Mouse Behavioral and Neuroendocrine Analysis Core Facility, Duke University Medical Center, Durham, NC 27710, USA
[6]Department of Biochemistry and Molecular Medicine, School of Medicine, University of California, Davis, Davis, CA, USA
[7]Center for Neuroscience, University of California, Davis, 1544 Newton Court, Davis, CA 95618, USA
[8]These authors contributed equally
[9]Lead contact
*Correspondence: deolson@ucdavis.edu (D.E.O.), lintian@ucdavis.edu (L.T.)
https://doi.org/10.1016/j.cell.2021.03.043

SUMMARY

Ligands can induce G protein-coupled receptors (GPCRs) to adopt a myriad of conformations, many of which play critical roles in determining the activation of specific signaling cascades associated with distinct functional and behavioral consequences. For example, the 5-hydroxytryptamine 2A receptor (5-HT2AR) is the target of classic hallucinogens, atypical antipsychotics, and psychoplastogens. However, currently available methods are inadequate for directly assessing 5-HT2AR conformation both *in vitro* and *in vivo*. Here, we developed psychLight, a genetically encoded fluorescent sensor based on the 5-HT2AR structure. PsychLight detects behaviorally relevant serotonin release and correctly predicts the hallucinogenic behavioral effects of structurally similar 5-HT2AR ligands. We further used psychLight to identify a non-hallucinogenic psychedelic analog, which produced rapid-onset and long-lasting antidepressant-like effects after a single administration. The advent of psychLight will enable *in vivo* detection of serotonin dynamics, early identification of designer drugs of abuse, and the development of 5-HT2AR-dependent non-hallucinogenic therapeutics.

INTRODUCTION

G protein-coupled receptors (GPCRs) represent attractive therapeutic targets with nearly 35% of all Food and Drug Administration (FDA)-approved medications (Hauser et al., 2017) affecting this class of proteins. Ligand-induced changes in GPCR conformation provide a structural basis for initiating intracellular signaling through heterotrimeric G proteins, arrestins, and other effectors (Kenakin and Miller, 2010). Biased ligands are capable of selectively activating or inactivating specific cellular pathways at the expense of others by stabilizing discrete GPCR conformational ensembles, and thus, have the potential to reduce undesirable side effects while maintaining efficacy (Roth et al., 2017; Shonberg et al., 2014).

Ligands for the 5-HT2AR were some of the first small molecules to demonstrate biased agonism (Berg et al., 1998). Since that initial report, 5-HT2AR ligands have been shown to couple to a variety of signal transduction pathways via 5-HT2A monomers and heterodimers leading to distinct transcriptome profiles

and behavioral effects (Fribourg et al., 2011; González-Maeso et al., 2003, 2007, 2008; Schmid and Bohn, 2010; Schmid et al., 2008). Furthermore, 5-HT2AR ligands represent some of the most important drugs in neuropsychiatry, including atypical antipsychotics like clozapine, psychedelics such as lysergic acid diethylamide (LSD), and neural plasticity-promoting compounds known as psychoplastogens (Olson, 2018).

Mounting preclinical and clinical evidence suggests that psychedelics may prove useful for treating a variety of neuropsychiatric diseases including depression, post-traumatic stress disorder (PTSD), and substance use disorder (SUD) (Chi and Gold, 2020). However, it is currently unclear if the subjective effects of these drugs are necessary to ameliorate disease symptoms (Olson, 2020; Yaden and Griffiths, 2020). Like ketamine, psychedelics promote neural plasticity in key circuits relevant to mood, fear, and reward (Ly et al., 2018). Recent rodent studies using sub-hallucinogenic doses (Cameron et al., 2019) and non-hallucinogenic congeners (Cameron et al., 2021) suggest that the hallucinogenic effects of 5-HT2AR ligands may not be necessary
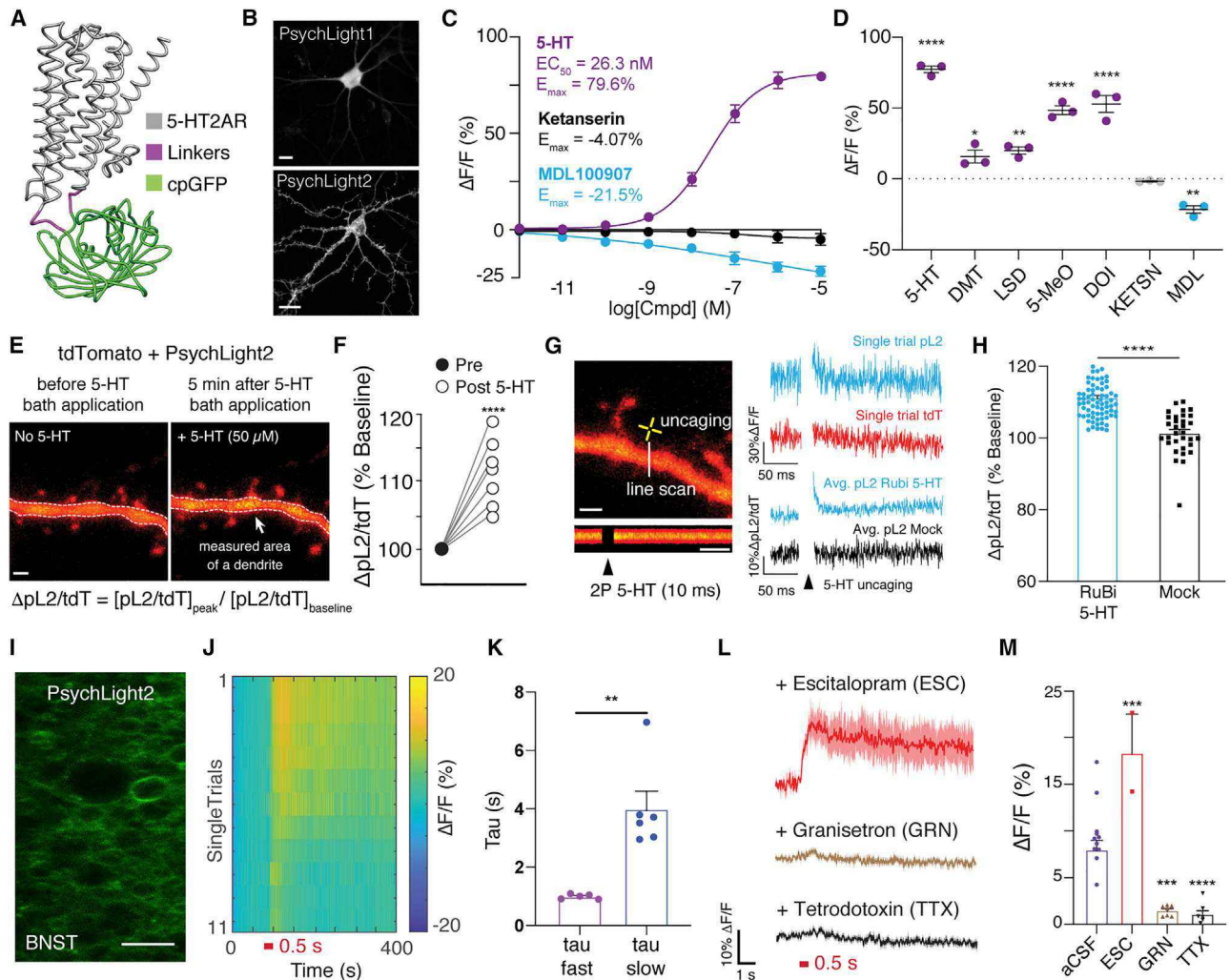
Figure 1. Development of a fluorescent sensor based on the 5-HT2A receptor

(A) Simulated structure of psychLight consisting of 5-HT2AR (gray), a linker (magenta) and a cpGFP (green).

(B) Representative images of cultured dissociated hippocampal neurons transiently expressing psychLight1 and psychLight2. Scale bar, 20 μm.

(C) PsychLight1-expressing HEK293T cells respond to ligands in a concentration-dependent manner.

(D) PsychLight1 is activated by hallucinogenic 5-HT2A ligands, but not non-hallucinogenic compounds when treated at 10 μM. ****$p < 0.0001$, **$p < 0.01$ and *$p < 0.05$, one-way ANOVA compared to KETSN with Dunnett's test.

(E and F) Two-photon imaging of cultured cortical slices expressing psychLight2 (pL2) following bath application of 5-HT.

(E) Representative images of a dendrite expressing psychLight2 (pL2) and tdTomato (tdT) before and after bath application of 50 μM 5-HT (imaged at 920 nm).

(F) Fluorescence intensity changes in pL2 were normalized to the tdT signal, (ΔpL2/tdT = 111.1% ± 1.8%, n = 7 region of interests [ROIs] from 4 cells; ****$p < 0.0001$, unpaired t test). Scale bar, 1 μm.

(G and H) Two-photon 5-HT uncaging evoked psychLight responses.

(G) Representative apical dendrites imaged during two-photon uncaging of serotonin. Representative single-trial traces of fluorescent intensity changes (ΔF/F%) of pL2 and tdT are shown in response to single pulse uncaging (10 ms). Averaged traces of ΔpL2/tdT in response to uncaging of Rubi-5HT (bottom) and without were shown. Scale bars, 1 μm.

(H) Characterization of peak response of green to red ratio (ΔpL2/tdT) normalized to the baseline for pL2 in response to single-pulse uncaging with and without RuBi-5-HT (ΔpL2/tdT = 111.2% ± 0.7%, n = 76 ROIs from 11 cells (Rubi-5-HT); 101.3% ± 1.0% n = 32 ROIs from 6 cells [mock 2P]), ****$p < 0.0001$, unpaired t test.

(I–K) Two-photon imaging of endogenous 5-HT release triggered by electrical stimuli in acute slices.

(I) A representative two-photon image of BNST acute slice expressing psychLight2. Scale bar, 50 μm.

(J) Single-trial response of psychLight2 to electrical stimuli (0.5 s, 4 V, 40 Hz, 20 pulses).

(K) The averaged off-kinetics of two groups of ROIs exhibiting fast and slow off rates. (40 pulses: Tau$_{fast}$ = 0.997 ± 0.0376 s, n = 5 trials; Tau$_{slow}$ = 3.998 ± 0.6103 s, n = 6 trails), **$p < 0.01$, unpaired t test.

(L) Averaged-trial traces of psychLight2 in response to electrical stimuli in the presence of escitalopram (ESC, 50 μM), granisetron (GRN, 10 μM), and tetrodotoxin (TTX,1 μM). Shaded area represents SEM.

to promote neural plasticity and produce therapeutic outcomes. Thus, there is a critical need to develop methods for reliably determining if a novel ligand is likely to induce hallucinogen-specific conformations of the 5-HT2AR.

Recent breakthroughs in the structural determination of ligand-activated GPCRs and GPCR-transducer complexes have significantly increased our understanding of how receptor activation leads to coupling with various signal transducers (Hilger et al., 2018; Kim et al., 2020; Roth et al., 2017). Although traditional methods for assessing GPCR activation have relied on the quantification of downstream signaling molecules (e.g., cyclic AMP [cAMP], Ca^{2+}, etc.), ligand-induced conformational changes are increasingly being exploited to develop fluorescence- and bioluminescence-based assays for measuring the recruitment of various transducers (Olsen et al., 2020; Wan et al., 2018). Although these methods have proven useful for understanding important details of GPCR activation related to kinetics and specific drug responses, the direct measurement of behaviorally relevant GPCR conformations in real time and *in vivo* is still challenging with current technologies. As a result, there are currently no assays capable of directly measuring hallucinogenic potential across a wide range of structurally diverse 5-HT2AR ligands.

Recently, we reported a modular strategy for creating genetically encoded fluorescent sensors that are activated by ligand-induced conformational changes in GPCRs (Patriarchi et al., 2018). Here, we applied this design strategy to develop psychLight, a 5-HT2AR-based fluorescent biosensor capable of detecting endogenous serotonin (5-HT) release in awake, behaving animals as well as conformations induced by hallucinogenic ligands *in vivo* and in a medium-throughput functional assay. By screening a small library of compounds, we successfully used psychLight to identify previously unknown hallucinogenic drugs and a non-hallucinogenic psychedelic analog with neural plasticity-promoting and antidepressant properties similar to the state-of-the-art fast-acting antidepressant ketamine (Table S1).

RESULTS

Development of psychLight
To develop a sensor capable of reporting ligand-induced conformations of the human 5-HT2AR, we replaced the third intracellular loop (IL3) of the 5-HT2AR with a circularly permuted green fluorescent protein (cpGFP) inserted between Lys263 and Ser316 (Figure S1A). The dynamic range in response to the endogenous ligand 5-HT was maximized by screening linker compositions between cpGFP and 5-HT2AR, optimizing the insertion site of cpGFP, and introducing key point mutations (Figure S1B) (Patriarchi et al., 2018). We named the top-performing variant psychLight1 (Figure 1A). To further improve membrane localization in neurons, we fused an endoplasmic reticulum (ER) export motif (FCYENEV) (Stockklausner et al., 2001) to the C terminus of psychLight1, yielding a version (i.e., psychLight2)

with improved membrane expression in both HEK293T cells and neurons (Figures 1B, S1C, and S1D).

We next investigated the pharmacological responses of the sensor. When psychLight1 is expressed in HEK293T cells, 5-HT activates the sensor with a half maximal effective concentration comparable to values obtained using assays designed to measure G protein and β-arrestin activation (Wacker et al., 2017) (Figure 1C). Moreover, other agonists were able to effectively increase the sensor's fluorescence intensity to varying degrees (Figure 1D). In contrast, the traditional 5-HT2AR antagonists ketanserin and MDL100907 either had minimal effect on psychLight1 fluorescence or slightly quenched the sensor (Figures 1C and 1D), and ketanserin was able to block 5-HT-induced activation of psychLight in HEK293T cells (Figures S2A and S2B). Taken together, these findings demonstrated that psychLight can convert ligand-induced conformational changes of the 5-HT2AR into fluorescence readouts, suggesting that psychLight may be uniquely suited for detecting specific conformations of the receptor induced by ligands.
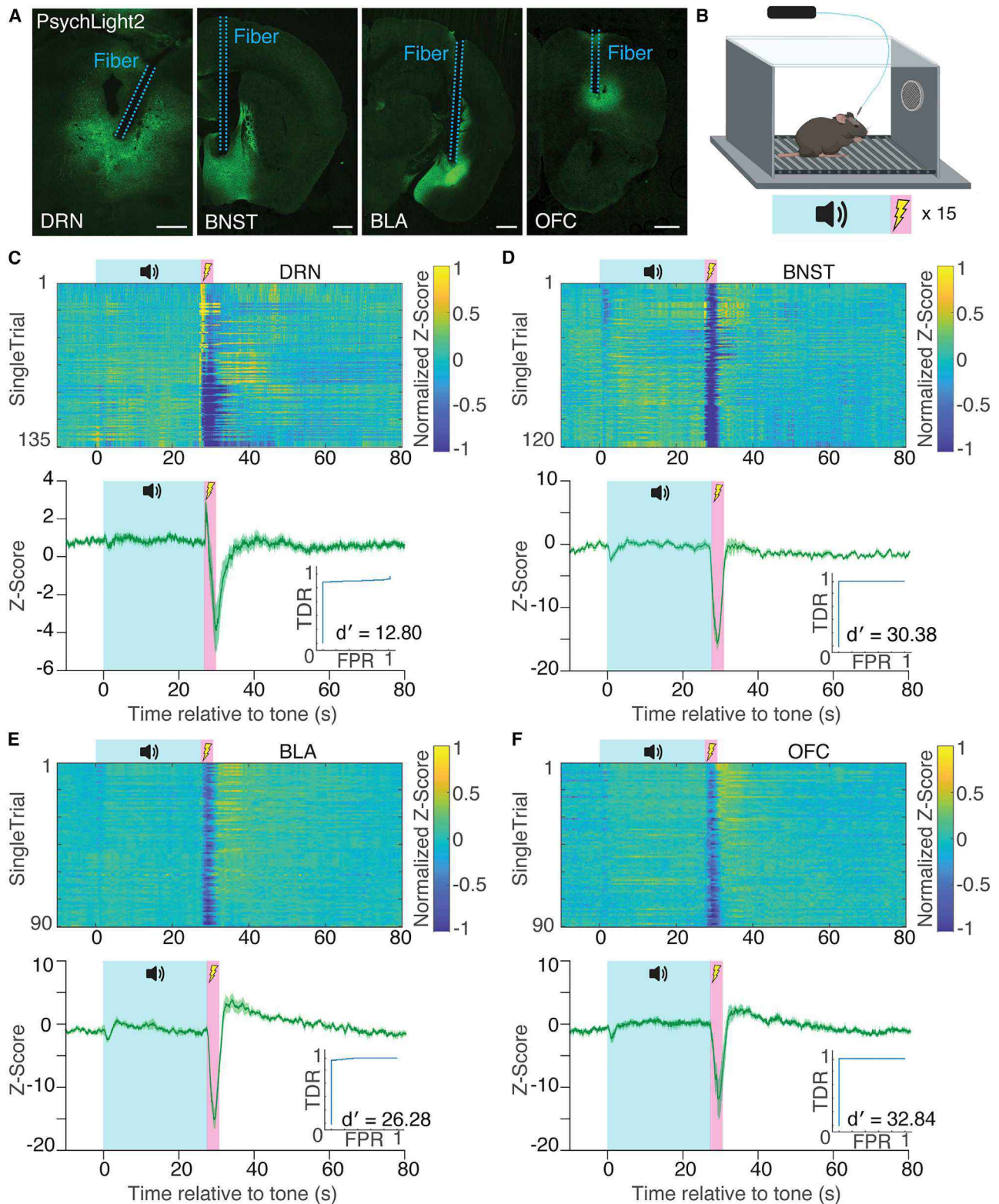
Two-photon imaging of endogenous serotonin dynamics *ex vivo* and *in vivo*
To assess the utility of psychLight2 for measuring endogenous serotonin transients, we characterized the sensitivity and kinetics of the sensor using two-photon imaging in cultured and acute brain slices. Approximately 3 weeks after infection with AAV9.*hSynapsin1*.psychLight2 into organotypic cortical slice cultures and biolistic transfection of a red cell-fill fluorescent protein, tdTomato, we imaged layer 2/3 pyramidal neurons using two-photon time-lapse imaging and line-scan acquisition mode (~3.3 lines/ms). Bath application of 5-HT (50 μM) led to a significant increase in the ratio of green (psychLight2 signal; pL2) to red (tdTomato signal; tdT) fluorescence intensities (Figures 1E and 1F). Focal uncaging of RuBi-5-HT at apical dendrites (single 10-ms pulse at 810 nm) evoked a rapid increase in psychLight fluorescence that returned to baseline within milliseconds (Tau_{off} = 5.4 ± 0.9 ms) (Figures 1G and 1H). In contrast, no increase in fluorescence was observed in response to a mock stimulus.

Next, we examined the ability of psychLight2 to report time-dependent changes in 5-HT dynamics using an acute slice preparation. Three weeks after injection of AAV9.*hSynapsin1*.psychLight2 into the bed nucleus of the stria terminalis (BNST) (Figure 1I), we performed two-photon imaging in frame-scan mode (33 Hz) and triggered endogenous 5-HT release by electrical stimulation. The sensitivity of psychLight2 was sufficient to detect electrically evoked 5-HT release in single trials (d' = 234.2, see STAR Methods for details) (Figure 1J). Interestingly, we noticed two types of responses that differed in their amplitudes and decay rates (ΔF/F = 4.7% ± 1.5%, Tau_{off} fast = 0.997 ± 0.038 s and ΔF/F = 9.7% ± 1.2%, Tau_{off} slow = 3.998 ± 0.610 s) (Figures 1J and 1K). The amplitude of the psychLight2 response could be enhanced by incubation with 50 μM

(M) Peak fluorescence changes in the absence (aCSF, n = 11 trials from 3 mice) and presence of compounds (ESC, n = 2 trials from 3 mice, ***p = 0.0002; GRN, n = 8 trials from 3 mice, ****p < 0.0001; TTX n = 9 trials from 3 mice, 40 pulses, one-way ANOVA compared to aCSF with Sidak's test). Data are represented by mean ± SEM.
See also Figures S1 and S2A–S2D and Tables S1 and S2.

Figure 2. PsychLight enables the detection of endogenous serotonin dynamics during fear conditioning using fiber photometry

(A) Expression of psychLight2 in the DRN, BNST, BLA and OFC near the location of fiber implantation. Scale bars, 500 μm.

(B) Schematic illustrating the design of auditory fear conditioning experiments (30-s tone co-terminating with a 1.5-s foot shock, n = 15 presentations).

escitalopram, a blocker of the 5-HT transporter (SERT) (ΔF/F = 18.4% ± 4.3%) (Figure 1L). Importantly, application of either the 5-HT$_3$ receptor antagonist granisetron (10 μM) (Ko et al., 2016), the sodium channel blocker tetrodotoxin (1 μM), or ketanserin (10 μM) was sufficient to block psychLight fluorescence in response to electrically-evoked 5-HT transients (Figures 1L, 1M, S2C, and S2D).

To determine if psychLight2 could measure 5-HT dynamics *in vivo*, we employed a fear conditioning paradigm coupled with fiber photometry in freely behaving mice. First, AAV.*hSynapsin1*.psychLight2 was injected into the BNST, the basolateral amygdala (BLA), the dorsal raphe nucleus (DRN), or the orbitofrontal cortex (OFC) along with implantation of an optical fiber (Figure 2A). After 2–3 weeks to allow full expression of the sensor, we measured 5-HT transients during an auditory fear conditioning experiment consisting of 15 presentations of a 30-s tone co-terminating with a 1.5-s foot-shock (0.5 mA) (Figure 2B). In the DRN, we observed a robust increase in fluorescence intensity immediately after the onset of foot-shock (Figure 2C), followed by a sharp decline during the shock. These results are consistent with Ca^{2+} transients recorded in the DRN using GCaMP6 during auditory fear conditioning (Ren et al., 2018). In the BNST, we observed an immediate decrease in fluorescence following foot-shock that returned to baseline within 4 s (Figure 2D). A similar initial reduction in fluorescence was observed in both the BLA and OFC; however, in these brain regions, the initial decrease in sensor activity was followed by a considerable rise in the fluorescence signal following the shock (Figures 2E and 2F). Serotonin dynamics were reliably detected across individual trials of the fear conditioning experiments (*d′* = 12.80, 30.38, 26.28, and 32.84 for the DRN, BNST, BLA, and OFC, respectively). To further demonstrate that changes in psychLight fluorescence during fear conditioning are specific to endogenous 5-HT2AR ligands, we injected AAV.*hSynapsin1*.psychLight0 into all four brain regions. PsychLight0 has a key point mutation (D155A) that completely prevents agonist binding. Unlike experiments using psychLight2, we did not observe significant changes in psychLight0 fluorescence following foot-shock (Figures S2E and S2F), indicating that psychLight2 detects endogenous agonists in freely behaving animals.

PsychLight activity differentiates hallucinogenic and non-hallucinogenic drugs

We next sought to determine if the sensor could faithfully report 5-HT2AR activation *in vivo* following systemic administration of an exogenous agonist. We chose to use 5-methoxy-*N*,*N*-dimethyltryptamine (5-MeO-DMT or 5-MeO), because it produces a robust head-twitch response (HTR) (Dunlap et al., 2020)—a mouse behavior induced by hallucinogenic 5-HT2AR ligands (Halberstadt et al., 2020; Hanks and González-Maeso, 2013). Three weeks after injection of AAV9.*hSynapsin1*.psychLight2 into the prelimbic cortex, we administered 5-MeO-DMT

(50 mg/kg, intraperitoneal [i.p.]) and measured psychLight2 response using fiber photometry (Figures 3A and 3B). Within 1 min of drug administration, we observed a sharp increase in fluorescence along with a concomitant increase in HTR. After several minutes, the psychLight signal stabilized and remained elevated while head twitch frequency decreased (Figure 3B). In contrast, when mice were administered vehicle or the 5-HT2AR antagonist ketanserin (KETSN, 4 mg/kg, i.p.), psychLight fluorescence remained unchanged or decreased, respectively (Figure 3C). These data suggest that psychLight is sensitive to both agonist- and antagonist-induced conformational changes *in vivo*.

We next assessed the sensor's ability to differentiate between known hallucinogenic agonists and structurally similar non-hallucinogenic analogs. We tested several pairs of hallucinogenic and non-hallucinogenic congeners representing the ergoline, tryptamine, and amphetamine classes of psychedelics. We chose these compounds because the propensity of these drugs to produce hallucinations in humans was known (Benes et al., 2006; Dunlap et al., 2018; Halberstadt et al., 2020; Kalir and Szara, 1963) or inferred from data using well-established rodent models of 5-HT2AR-induced hallucinations (Hanks and González-Maeso, 2013), such as rat drug discrimination (DD) (Glennon et al., 1983) and mouse HTR assays (Dunlap et al., 2020), which correlate exceptionally well with hallucinogenic potency in humans (Halberstadt et al., 2020).

All four hallucinogenic compounds activated psychLight1 when expressed in HEK293T cells, with half maximal effective concentrations ranging from 18.8–627 nM (LSD, EC$_{50}$ = 18.8 nM, E$_{max}$ = 20.0%; 5-MeO, EC$_{50}$ = 157 nM, E$_{max}$ = 48.4%; DOI, EC$_{50}$ = 35.5 nM, E$_{max}$ = 52.9%; and DMT, EC$_{50}$ = 627 nM, E$_{max}$ = 12.4%). In sharp contrast, none of the non-hallucinogenic congeners were able to increase the sensor's response, even at concentrations as high as 10 μM (Figures 3D–3G). By running the assay in antagonist mode, we were able to demonstrate that non-hallucinogenic compounds such as lisuride (LIS) and 6-MeO-DMT (6-MeO) are capable of binding to the receptor despite lacking efficacy (Figures S3A and S3B). The large E$_{max}$ differences between the hallucinogenic and non-hallucinogenic compounds within a given pair are remarkable given the extremely high degree of structural similarity between the paired molecules.

PsychLight1 potencies, but not efficacies, correlate exceptionally well with hallucinogenic potencies in humans (r^2 = 0.9) (Figure 3H). This strong correlation is noteworthy considering the error associated with estimating hallucinogenic potencies in humans and the fact that our cellular assay does not account for potential differences in pharmacokinetics. Furthermore, ligand activation of psychLight1 appears to be distinct from other measures of 5-HT2AR activation including phosphoinositide hydrolysis (Cussac et al., 2008), Gq activation (Rabin et al., 2002), and calcium mobilization (Cussac et al., 2008) (Figure 3I).

(C–F) Single-trial heatmap and averaged-trial traces of serotonin dynamics in DRN (C, n = 135 trials from 9 animals), BNST (D, n = 120 trials from 8 animals), BLA (E, n = 90 trials from 6 animals), and OFC (F, n = 90 trials from 6 animals) in response to a tone (blue) and foot shock (pink). ROC plots indicate true detection rate (TDR) against false-positive rate (FPR), and *d′* is calculated by avg(Z score$_{shock}$)/std(Z score$_{baseline}$). Average traces indicated by solid lines; shaded area represents SEM. DRN, dorsal raphe nucleus; BNST, bed nucleus of the stria terminalis; BLA, basolateral amygdala; OFC, orbitofrontal cortex.
See also Figures S2E and S2F and Tables S1 and S2.
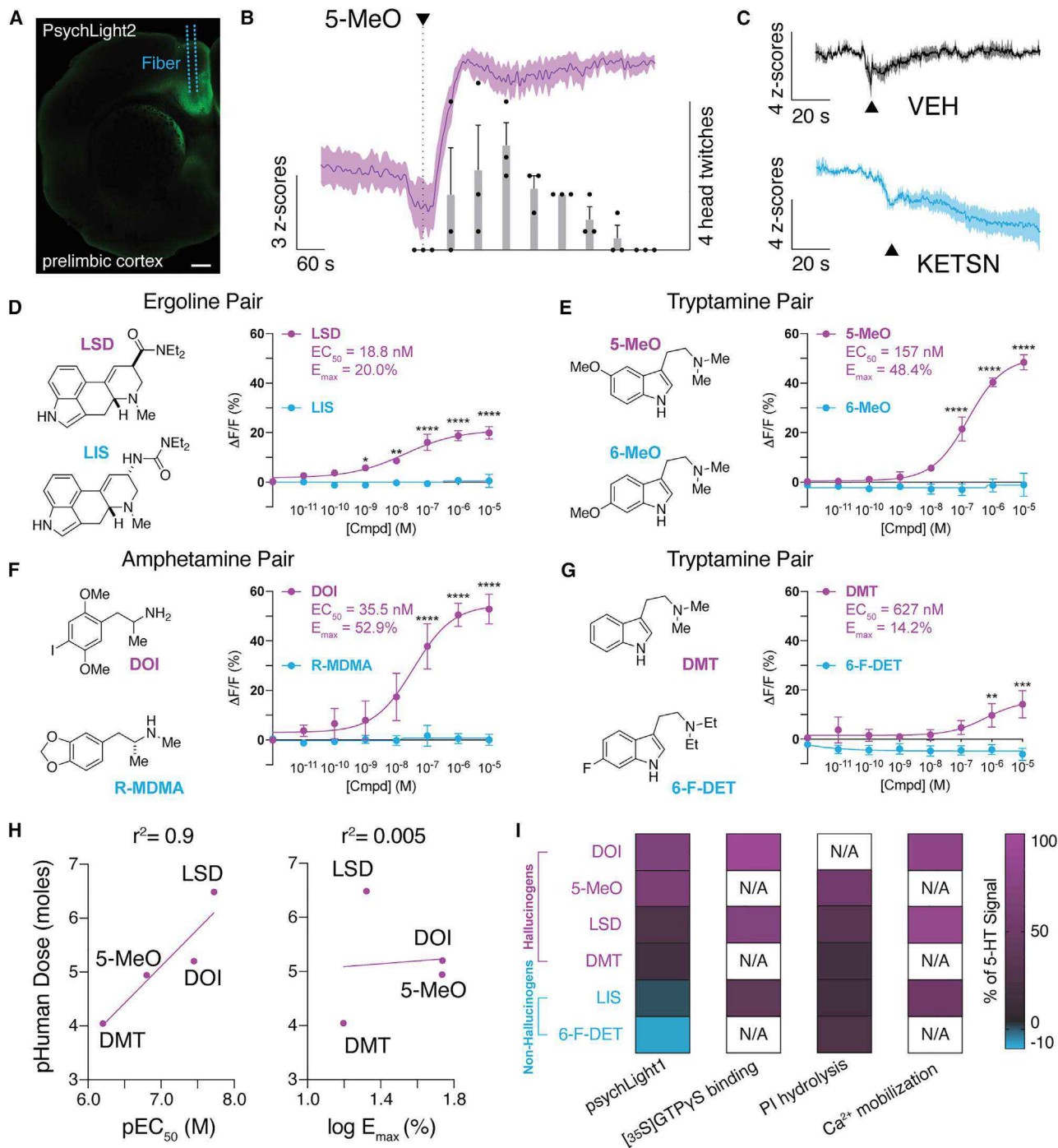
Figure 3. PsychLight is activated by hallucinogenic drugs *in vivo* and *in vitro*

(A–C) PsychLight2 *in vivo* responses to drugs as measured by fiber photometry.

(A) Expression of psychLight2 in the prelimbic cortex near the site of fiber implantation. Scale bar, 500 μm.

(B) Averaged-trial traces of psychLight2 responses shown as *Z* score following injection of 50 mg/kg 5-MeO (magenta, i.p.). The number of head-twitch responses (bars) were also recorded and binned into 1-min intervals (n = 3 animals).

(C) Averaged-trial traces of psychLight2 responses following the injection either of the saline (VEH; top black) or an antagonist (4 mg/kg KETSN, bottom blue, i.p.) (n = 3 animals). Average traces indicated by solid lines; shaded area represents SEM.

(D–G) Concentration-response studies using HEK293T cells transiently expressing psychLight1. Hallucinogens of the ergoline, tryptamine, and amphetamine classes of psychedelics (magenta) were tested along with their non-hallucinogenic congeners (blue). Hallucinogens activated psychLight1 while their

(legend continued on next page)

Development of a psychLight-based medium-throughput pharmacological assay

To enable medium-throughput identification of hallucinogenic designer drugs of abuse as well as non-hallucinogenic therapeutics targeting 5-HT2ARs, we developed a screening platform based on wide-field high content imaging of a HEK293T cell line stably expressing psychLight2 (PSYLI2) under the EF1α promoter (Figures 4A and S4A). Relative responses were similar using either a confocal microscope or high content imager (Figure S3C). A Z-factor (Zhang et al., 1999) was generated using serotonin and ketanserin as positive and negative controls, respectively (Z factor = 0.6, n = 42) (Figure S3D).

To assess the sensitivity of this assay, we first tested a panel of ligands with similar molecular structures to 5-HT (Figure 4B). We observed that subtle differences in ligand structure can significantly modulate the fluorescence signal generated by PSYLI2 cells (Figure 4C). Most notably, increasing N-methylation tends to reduce the magnitude of the sensor response (e.g., 5-HT: $\Delta F/F$ = 46.3% ± 1.4%; N-methylserotonin, N-5-HT: $\Delta F/F$ = 24.6% ± 1.7%; and N,N-dimethylserotonin, BUFO: $\Delta F/F$ = 22.3% ± 2.8%), which is consistent with a structure-activity relationship previously reported for 5-HT2AR-induced accumulation of [^{3}H]inositol phosphates (Ebersole et al., 2003). Surprisingly, the hydroxyl substituent of 5-HT does not appear to be necessary for achieving full agonism as tryptamine produces a robust response (Figure 4C).

Next, we screened a library of eighty-three compounds consisting of known hallucinogens (as defined by human data or predicted based on the mouse HTR and/or DD assays), known non-hallucinogenic 5-HT2AR ligands, psychoactive drugs with unknown 5-HT2AR affinity, and compounds from our medicinal chemistry program (Figures S4B, S4C, and S5; see STAR Methods for details). When the assay was performed in agonist mode (Figure 4D, abscissa), serotonergic hallucinogens reliably gave a response of greater than +1 SD from the vehicle control (Figures 4D and S4B). Non-hallucinogenic 5-HT2AR ligands did not activate the sensor in agonist mode but decreased fluorescence in antagonist mode (Figure 4D, ordinate). Compounds that do not bind to the 5-HT2AR did not produce a response in either agonist or antagonist mode.

When screened at 10 μM using PSYLI2 cells, 2-bromolysergic acid diethylamide (BOL-148) and bromocriptine produced unexpected fluorescence signals, because these compounds are widely believed to be non-hallucinogenic. Given that both compounds contain a two-bromoindole structural motif, we suspected that the inherent fluorescence of these molecules was resulting in false-positive signals. Therefore, we performed concentration-response experiments in PSYLI2 cells using a high content imager and under cell-free conditions using a fluorescence plate reader (Figure S4D). The results confirmed our hypothesis that the signal from BOL-148 and bromocriptine at 10 μM was due to the inherent fluorescence of these compounds, and not due to activation of the sensor.

By running the assay in both agonist and antagonist mode (i.e., 100 nM 5-HT with 10 μM test compound), we were able to distinguish between non-hallucinogenic ligands of the 5-HT2AR and compounds that do not bind to the receptor (Figures 4D, 4E, and S4C). We combined data from agonist and antagonist modes to define a "ligand score" (see STAR Methods for details); positive and negative ligand scores indicated likely hallucinogenic and non-hallucinogenic ligands of the 5-HT2AR, respectively, whereas values close to zero indicated compounds that were unlikely to be 5-HT2AR ligands (Figure 4E). For example, the ligand scores for LSD and lisuride were 23.0 and −42.3, respectively. In contrast, non-serotonergic hallucinogens/dissociatives such as salvinorin A, ketamine, and phencyclidine displayed ligand scores close to 0 (Figure 4E).

Finally, to further characterize the pharmacological profiles of non-hallucinogenic ligands, we performed Schild regression analysis for several compounds with negative ligand scores (Figures S6A–S6D). The pA2 values indicate that LIS, apomorphine, and benztropine are potent psychLight competitive antagonists, whereas 6-MeO is significantly less potent (Figures S6A–S6D).

PsychLight accurately predicts the hallucinogenic potentials of designer drugs

We next screened a small library consisting of thirty-four compounds with unknown hallucinogenic potentials (Figure 4E). By assessing ligand scores, we predicted that the smaller 5-F-DMT and 5-Cl-DMT would be hallucinogenic, while the larger 5-Br-DMT would not (Figures 4E and 5A). To confirm this prediction *in vivo*, we performed a three-point dose-response study measuring HTR (Figure 5B). As expected, both 5-F-DMT and 5-Cl-DMT produced robust HTRs, while 5-Br-DMT failed to induce HTRs at any dose (Figure 5B). Interestingly, the effects of the compounds on locomotion and the HTR were not correlated (Figure 5C). The 5-halo-DMT series really highlights the power of psychLight for detecting profound functional differences between compounds that share a high degree of structural similarity.

Next, we sought to use psychLight to identify non-hallucinogenic 5-HT2AR ligands occupying previously unknown chemical space. Because AAZ-A-154 (Figure 5A) had never been reported in the literature and exhibited a favorable ligand score, we subjected it to further testing. Schild regression analysis revealed that AAZ-A-154 functions as a psychLight competitive antagonist (Figure 5D). Using a panel of GPCR-based sensors (e.g., dopamine, adrenergic, opioid, and serotonin receptors)

---

non-hallucinogenic congeners did not. n = 3 cells from 3 different cell passages; Error bars represent SEM, *p < 0.05, **p < 0.01, ***p < 0.001, ****p < 0.0001, compared to the non-psychedelic drug, two-way ANOVA.

(H) PsychLight1 EC_{50} values, but not E_{max} values, correlate with hallucinogen potencies in humans.

(I) PsychLight1 E_{max} values differentiate hallucinogens and non-hallucinogens, but other measures of 5-HT2AR activation (e.g., phosphoinositide [PI] hydrolysis, Ca^{2+} mobilization, [^{35}S]GTPγS binding) do not. Data represented by the heatmap with a double color gradient from values above 0 (magenta to black) and data below 0 (black to blue). Data are normalized to 5-HT values within each experiment. Data for PI hydrolysis, Ca^{2+} mobilization, and [^{35}S]GTPγS binding were obtained from previous reports (Cussac et al., 2008; Rabin et al., 2002). PI hydrolysis data for 6-F-DET were estimated based on graphical data presented in Rabin et al. (2002). N/A indicates that the data are not available.

See also Figures S3A and S3B and Tables S1 and S2.
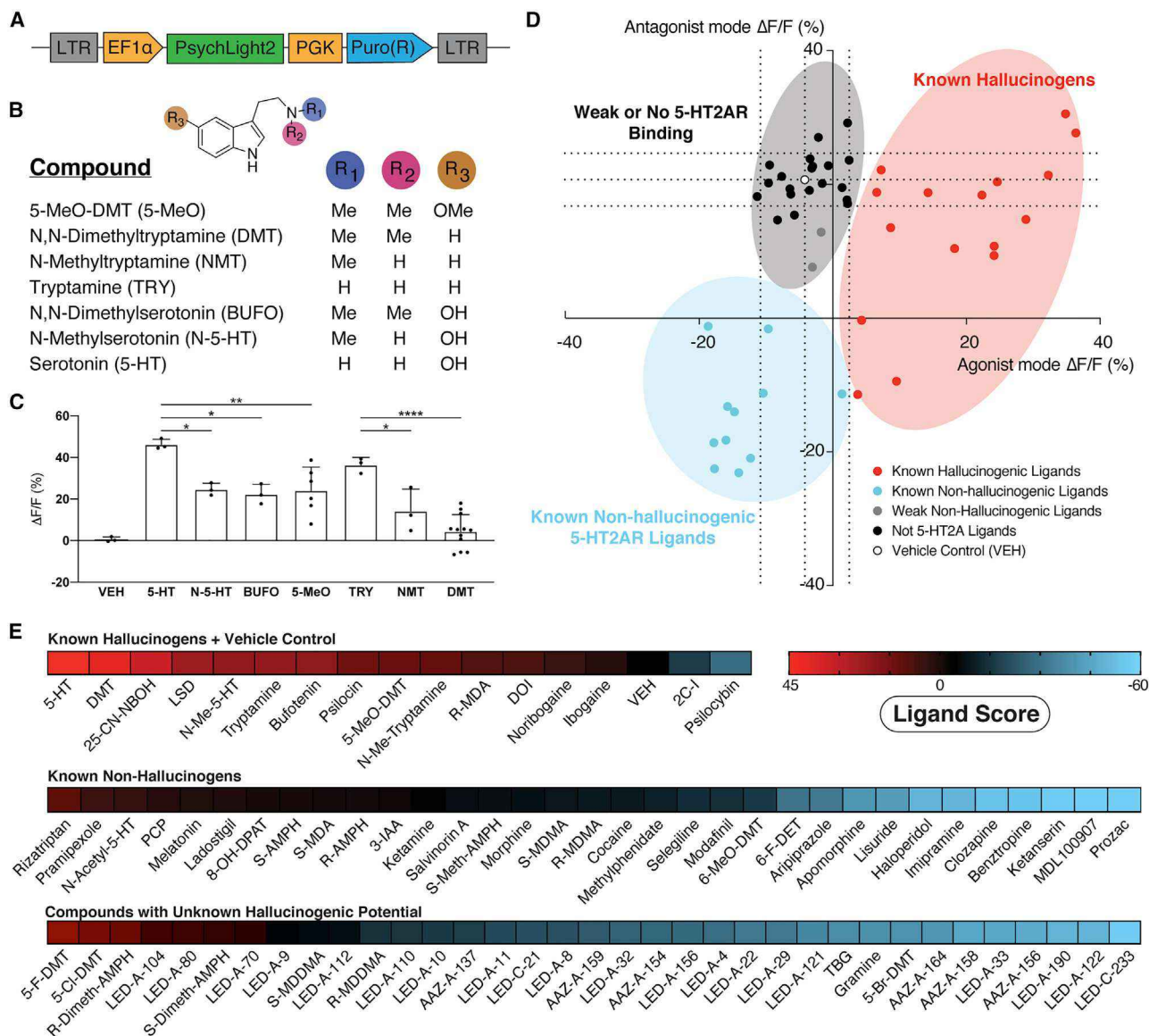
Figure 4. Development of a medium-throughput psychLight-based pharmacological assay

(A) A lentivirus expressing psychLight2 under the EF1α promoter was used to engineer a HEK293T cell line stably expressing psychLight2 (PSYLI2) (see STAR Methods for details).

(B and C) Structure-function studies using a variety of structurally related tryptamines.

(B) Structures of compounds.

(C) PSYLI2 fluorescence in response to compound treatments (10 μM). Data are represented by mean ± SEM, ****$p < 0.0001$, **$p < 0.01$ and *$p < 0.05$, one-way ANOVA multiple comparison with Tukey's test.

(D) A series of hallucinogenic and non-hallucinogenic compounds with known 5-HT2AR affinities were tested in agonist (abscissa) and antagonist (ordinate) modes. Dotted lines represent 1 SD from the VEH control (white). Hallucinogenic and non-hallucinogenic 5-HT2AR ligands are shown in red and blue, respectively. Compounds with weak affinity for the 5-HT2AR (∼1–10 μM) are shown in gray, whereas compounds that are known to not bind to the 5-HT2AR are shown in black. Dots indicate averaged ΔF/F values (n = 3 replicates from 3 passages of cells).

(E) Heatmap of ligand scores (see STAR Methods for details). Ligand scores greater than 0 indicate compounds more likely to be hallucinogenic while scores less than 0 indicate compounds that are more likely to be non-hallucinogenic ligands of the 5-HT2AR.

See also Figures S3C, S3D, S4, S5, and S6A–S6D and Tables S1 and S2.

(Patriarchi et al., 2018; Wan et al., 2021) in both agonist and antagonist mode, we observed that AAZ-A-154 exhibits high selectivity for 5-HT2 receptors (Figure S6E). To assess the hallu-

cinogenic potential of AAZ-A-154 in vivo, we performed HTR experiments across multiple doses in mice. As expected, AAZ-A-154 failed to produce any head-twitches, even up to doses as
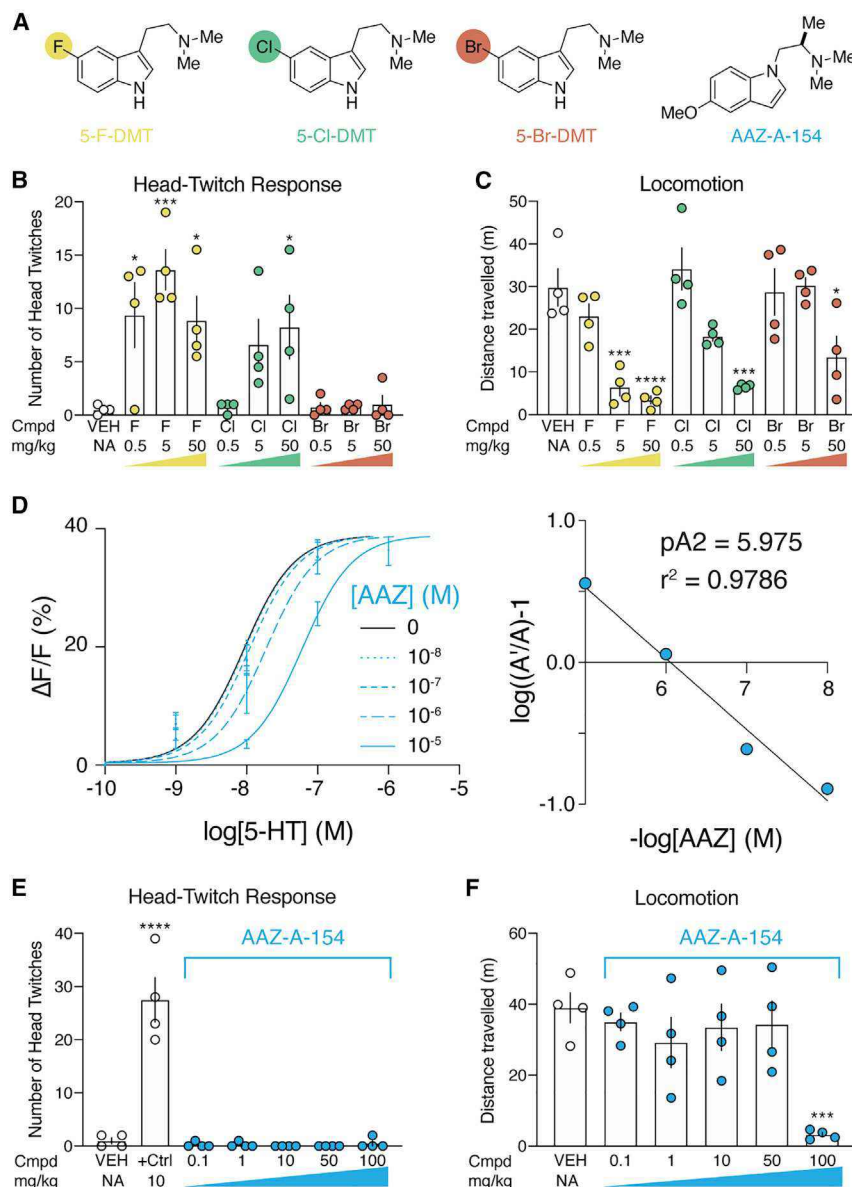
Figure 5. PsychLight accurately predicts hallucinogenic potentials of previously untested compounds

(A) Structures of 5-halo-DMT derivatives and AAZ-A-154. Colored circles indicate the relative size of the halogen atom compared to each other.

(B) Both 5-F-DMT and 5-Cl-DMT produce positive ligand scores and induce head-twitches in mice. In contrast, 5-Br-DMT produces a negative ligand score and does not induce a HTR (n = 4 mice).

(C) All 5-halo-DMTs produce dose-dependent decreases in locomotion (n = 4 mice).

(D) Schild regression analysis reveals that AAZ-A-154 is a psychLight competitive antagonist (n = 3 replicates from 1 passage of cells).

(E) AAZ-A-154 does not trigger a HTR at any dose compared to that triggered by 5-MeO-DMT (n = 4 mice).

(F) AAZ-A-154 only decreases locomotion at a very high dose (100 mg/kg) (n = 4 mice). Data are represented as mean ± SEM. ****$p < 0.0001$, ***$p < 0.001$, and *$p < 0.05$, versus the vehicle control, one-way ANOVA with Dunnett's test.

See also Figure S6E and Tables S1 and S2.

gesting that AAZ-A-154 triggers dendritic growth through activation of 5-HT2Rs.

Hallucinogenic and dissociative psychoplastogens, are known to produce both rapid and sustained antidepressant effects (Olson, 2018). Because AAZ-A-154 is not predicted to produce hallucinations (Figures 4E and 5E), we were interested in assessing its antidepressant potential *in vivo* using behavioral assays relevant to active stress-coping strategies (i.e., forced swim test) and anhedonia (i.e., sucrose preference).
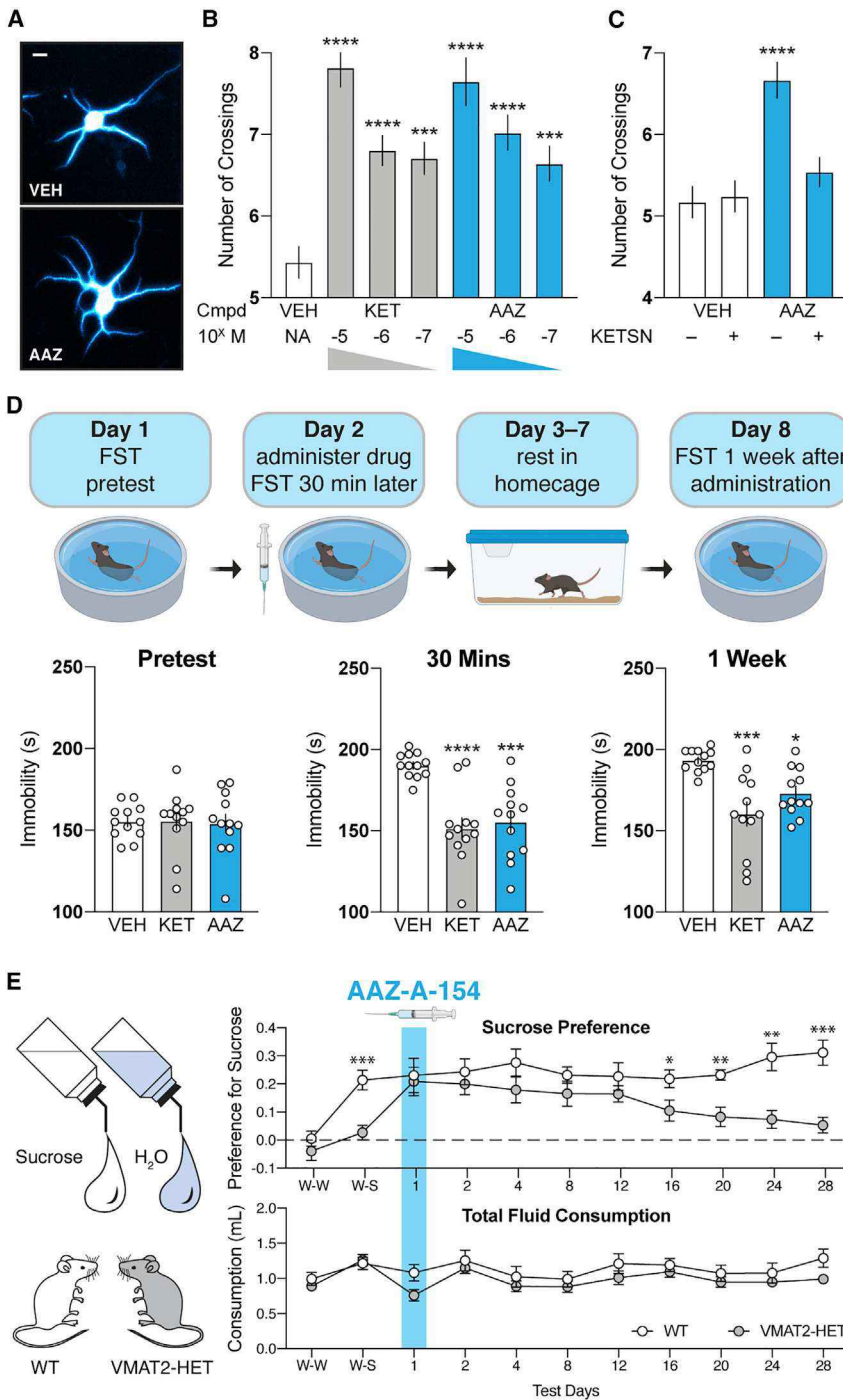
AAZ-A-154 decreased immobility in the forced swim test (FST) (Figure 6D)—an effortful behavioral response commonly produced by other known psychoplastogens (Cameron et al., 2018) and antidepressants such as ketamine (Li et al., 2010). In

high as 100 mg/kg (Figure 5E). However, a high dose of AAZ-A-154 decreased locomotion (Figure 5F), indicating that this compound can still impact behavior without producing hallucinogenic effects.

Characterizing the antidepressant-like effects of AAZ-A-154

Given its similar structure to several known psychoplastogens (Ly et al., 2018), we tested the ability of AAZ-A-154 to promote dendritic outgrowth in cultured rat embryonic cortical neurons (Cameron et al., 2021; Dunlap et al., 2020). Treatment with AAZ-A-154 increases dendritic arbor complexity to a comparable extent as the fast-acting antidepressant ketamine (KET) (Figures 6A and 6B). This psychoplastogenic effect was abolished by the 5-HT2R antagonist ketanserin (KETSN) (Figure 6C), sug-

these studies, we utilized C57BL/6J mice, because this strain does not respond robustly to traditional antidepressants such as selective serotonin reuptake inhibitors (SSRIs) or tricyclics (Hascoët and Bourin, 2009), thus highlighting the similarity between AAZ-A-154 and next-generation antidepressants like ketamine. AAZ-A-154 produced both rapid (30 min) and long-lasting (1 week) antidepressant-like effects after a single administration (Figure 6D).

To determine if AAZ-A-154 could ameliorate anhedonia, we used VMAT2 heterozygous (VMAT2-HET) mice. We chose this animal model of depression because pharmacological inhibition of VMAT2 precipitates depressive-like behaviors in humans, and VMAT2-HET mice display several depressive phenotypes including a reduced preference for a 1% sucrose solution over water alone (Fukui et al., 2007). At baseline, the wild-type (WT)

Figure 6. A predicted non-hallucinogenic compound with antidepressant potential

(A) Representative images demonstrating that AAZ-A-154 promotes dendritic branching. Scale bar, 20 μm.

(B) Maximal number of crossings (N_{max}) from Sholl plots (n = 51–60 neurons). ****$p < 0.0001$, ***$p < 0.001$, one-way ANOVA with Dunnett's test.

(C) The effects of AAZ (100 nM) on dendritic growth can be blocked by the 5-HT2R antagonist ketanserin (KETSN, 1 μM, n = 39–58 neurons). ****$p < 0.0001$, one-way ANOVA with Dunnett's test.

(D) Schematic depicting the forced swim test design. AAZ-A-154 (20 mg/kg) produces fast (30 min) and long-lasting (1 week) antidepressant-like effects in the FST comparable to ketamine (KET) (n = 12). ****$p < 0.0001$, ***$p < 0.001$, and *$p < 0.05$, one-way ANOVA with Dunnett's test.

(E) Sucrose preference test reveals that AAZ (15 mg/kg) reduces anhedonia in VMAT2-HET mice for at least 12 days. W-W, water-water pairing; W-S, water-sucrose (1%) pairing. When given the choice between water and a 1% sucrose solution (W-S), only WT mice displayed a sucrose preference. Total fluid consumption was not different between genotypes at any time point. n = 11 mice/genotype; data are represented as means and SEMs, **$p < 0.01$ and *$p < 0.05$, WT versus VMAT2-HET, repeated-measures ANOVA with Bonferroni corrected pairwise comparisons.

See also Tables S1 and S2.

VMAT2-HET mice cannot be attributed to differential fluid consumption because both genotypes drank similar volumes of liquids across the entire experiment (Figure 6E). Moreover, the effects of AAZ-A-154 cannot be ascribed to increasing sucrose palatability, because AAZ-A-154 did not modify sucrose preference in the WT animals (Figure 6E). Taken together, these results suggest that psychLight can be used to identify both hallucinogenic and non-hallucinogenic ligands of the 5-HT2AR.

DISCUSSION

We developed psychLight as a 5-HT2AR-based fluorescent sensor capable of measuring endogenous 5-HT dynamics and detecting hallucinogenic conformations of the receptor. PsychLight exhibits millisecond off kinetics, which enabled us to detect time-dependent release/reuptake of 5-HT *ex vivo* and *in vivo*. Interestingly, we observed both fast and slow decaying 5-HT signals in acute BNST slices following electrical stimulation. However, it is unclear what causes the differential 5-HT time courses, although an SSRI can increase the amplitude of the response and slow reuptake. Compared to iSeroSnFR (Unger et al., 2020), psychLight displayed a much

animals displayed a strong preference for the sucrose solution whereas the VMAT2-HET mice did not (Figure 6E). However, immediately following a single administration of AAZ-A-154, the VMAT2-HET mice exhibited a sucrose preference that was indistinguishable from WT controls. This anti-anhedonic effect persisted for at least 12 days before the treated VMAT2-HET animals began to display reduced sucrose preference (Figure 6E). Notably, the change in sucrose preference observed for the

higher apparent affinity even with a relatively smaller dynamic range. These intrinsic properties may make psychLight extremely useful for reporting low concentration events, although psychLight is likely to become fully saturated following a massive release of 5-HT. Together with existing genetically encoded indicators (Unger et al., 2020; Wan et al., 2021), we anticipate that psychLight will prove essential for fully understanding the effects of endogenous 5-HT on brain function. Future side-by-side comparisons of the sensors' properties under identical experimental conditions across various species will provide useful information to guide which sensor to choose for a particular *in vivo* application.

Unlike existing serotonin sensors, psychLight is based on the 5-HT2AR, which plays an essential role in the hallucinogenic effects of psychedelics. Thus, the fluorescence changes of psychLight correlate with ligand-induced conformational changes specific to serotonergic hallucinogens. This is a unique feature of psychLight compared to other 5-HT sensors. In fact, iSeroSnFR exhibits low affinity for many hallucinogenic 5-HT2AR ligands (Unger et al., 2020). In principle, extensive binding pocket engineering of iSeroSnFR could produce a sensor specific for a single hallucinogenic compound, but such a sensor would not be generalizable to the broad class of structurally diverse serotonergic hallucinogens. PsychLight solves this issue by directly measuring conformational changes of the 5-HT2AR—a receptor that is activated by a wide range of diverse serotonergic hallucinogens including tryptamines, ergolines, and amphetamines. This direct measurement of 5-HT2AR conformational change overcomes the limitations of existing methods, which either provide a snap-shot view of the interaction or depend on slow, indirect secondary signaling (González-Maeso et al., 2007). However, to fully understand the action of biased 5-HT2AR ligands at the molecular level, the structures of psychLight bound to activating and inactivating ligands will be essential. Determining the spatial and temporal kinetics of ligand-receptor interactions and correlating this information to downstream signaling will provide additional insight into ligands' molecular and cellular mechanisms of action.

PsychLight fills the gap between *in vitro* testing of novel compounds and *in vivo* behavioral studies. To date, labor-intensive and costly rodent HTR and DD assays have been the most commonly used methods to assess the hallucinogenic potentials of novel compounds (Halberstadt et al., 2020). González-Maeso et al. (2007) have demonstrated that hallucinogenic and non-hallucinogenic 5-HT2AR ligands induce distinct immediate early gene expression patterns and may differentially activate 5-HT2AR-mGluR2 heterodimers (González-Maeso et al., 2007, 2008). However, these results have yet to be developed into a reliable cellular assay capable of differentiating between hallucinogenic and non-hallucinogenic congeners across a wide range of chemical structures. Using psychLight, hallucinogenic potential can be rapidly assessed in cells through direct fluorescence readout, enabling the identification of potential hallucinogens at an early stage in the drug discovery process. We predict that this assay will be easily adapted to a 384-well format and will complement additional orthogonal GPCR assays (e.g., Ca^{2+} flux, G protein activation, β-arrestin activation, cAMP production, etc.).

PsychLight can be used to identify non-hallucinogenic 5-HT2AR antagonists (e.g., antipsychotics like clozapine) or non-hallucinogenic biased agonists (e.g., LIS). Non-hallucinogenic psychoplastogens have emerged as an incredibly exciting class of 5-HT2AR ligands given the broad implications that neural plasticity-promoting compounds have for treating a variety of brain disorders (Cameron et al., 2021; Dunlap et al., 2020). We used psychLight to identify AAZ-A-154—a non-hallucinogenic analog of a psychedelic compound occupying previously unknown chemical space that promotes neuronal growth and produces long-lasting (>2-week) beneficial behavioral effects in rodents following a single administration. Tabernanthalog (TBG) is the only other known non-hallucinogenic psychoplastogen with antidepressant-like properties (Cameron et al., 2021), and TBG has a similar ligand score as AAZ-A-154 (Figure 4E). *In vivo*, it appears that AAZ-A-154 may be more potent than TBG while producing more sustained antidepressant effects.

To date, the precise mechanisms of action of hallucinogens at molecular and circuit levels remain largely unknown (Aghajanian and Marek, 1999; Preller et al., 2018). Genetic tools including reporters, sensors, and effectors that enable the monitoring and manipulation of neuronal activity will be useful for dissecting the circuits involved in hallucinogenic versus antidepressant effects. Furthermore, the identification of functionally selective GPCR ligands will be key to the advancement of future therapeutics targeting this class of receptors. The development of psychLight outlines a general strategy for achieving this goal by directly measuring distinct, behaviorally relevant, ligand-induced conformational changes.

Limitations of study

This study has a number of limitations that should be addressed by follow-up experiments. Although psychLight can predict hallucinogenic potential, the mechanisms underlying the effects of 5-HT2AR ligands at molecular, cellular, and circuit levels are still opaque. A critical step to understand the molecular mechanisms of 5-HT2AR ligands will be to obtain and compare structures of psychLight bound to hallucinogenic and non-hallucinogenic ligands. Future work will need to rely on a combination of tools (e.g., imaging, electrophysiology, and behavior) to better understand the molecular and circuit level mechanisms that give rise to hallucinogenic and antidepressant effects. Second, although psychLight provides direct examination of the conformational changes induced by biased 5-HT2AR ligands, the relationships between psychLight signals and other assays measuring downstream signaling have not been established. A detailed understanding of these relationships will be essential to reveal the mechanistic actions of biased ligands. Finally, a full pharmacological profile of AAZ-A-154 should be obtained and include information on mechanism of action, off-target effects, pharmacokinetics, full dose-response studies, potential toxicity, and efficacy validated using other established assays.

STAR★METHODS

Detailed methods are provided in the online version of this paper and include the following:

SUPPLEMENTAL INFORMATION

Supplemental information can be found online at https://doi.org/10.1016/j.cell.2021.03.043.

ACKNOWLEDGMENTS

AUTHOR CONTRIBUTIONS

D.E.O. and L.T. conceived the project, supervised its execution, and assisted with data analysis. C.D. developed psychLight1 and psychLigth2 and engineered PSYLI2. C.D. and C.L. designed the assay and screened the compounds. L.E.D. and A.A. synthesized the compounds in the medicinal chemistry library. C.D., C.L., and L.E.D. performed the HTR experiments for the halo-DMTs. M.V.V. performed the FST and HTR experiments for AAZ-A-154. W.C.W. supervised the sucrose preference experiments in the VMAT2-HET mice and the statistical analyses. W.C.O. and I.-W.H. performed the two-photon uncaging experiments. J.S. performed *ex vivo* recording. CD performed the fiber photometry experiments. C.D., C.L., L.E.D., D.E.O., and L.T. wrote the manuscript with input from W.C.O. and W.C.W.

DECLARATION OF INTERESTS

INCLUSION AND DIVERSITY

We worked to ensure sex balance in the selection of non-human subjects. One or more of the authors of this paper self-identifies as an underrepresented ethnic minority in science. The author list of this paper includes contributors from the location where the research was conducted who participated in the data collection, design, analysis, and/or interpretation of the work.

REFERENCES

Aghajanian, G.K., and Marek, G.J. (1999). Serotonin and hallucinogens. Neuropsychopharmacology *21* (2, Suppl), 16S–23S.

Benes, H., Deissler, A., Rodenbeck, A., Engfer, A., and Kohnen, R. (2006). Lisuride treatment of restless legs syndrome: first studies with monotherapy in de novo patients and in combination with levodopa in advanced disease. J. Neural Transm. (Vienna) *113*, 87–92.

Berg, K.A., Maayani, S., Goldfarb, J., Scaramellini, C., Leff, P., and Clarke, W.P. (1998). Effector pathway-dependent relative efficacy at serotonin type 2A and 2C receptors: evidence for agonist-directed trafficking of receptor stimulus. Mol. Pharmacol. *54*, 94–104.

Blair, J.B., Kurrasch-Orbaugh, D., Marona-Lewicka, D., Cumbay, M.G., Watts, V.J., Barker, E.L., and Nichols, D.E. (2000). Effect of ring fluorination on the pharmacology of hallucinogenic tryptamines. J. Med. Chem. *43*, 4701–4710.

Broussard, G.J., Unger, E.K., Liang, R., McGrew, B.P., and Tian, L. (2018). Imaging Glutamate with Genetically Encoded Fluorescent Sensors. In Biochemical Approaches for Glutamatergic Neurotransmission, S. Parrot and L. Denoroy, eds. (Springer New York), pp. 117–153.

Cameron, L.P., Benson, C.J., Dunlap, L.E., and Olson, D.E. (2018). Effects of N, N-Dimethyltryptamine on Rat Behaviors Relevant to Anxiety and Depression. ACS Chem. Neurosci. *9*, 1582–1590.

Cameron, L.P., Benson, C.J., DeFelice, B.C., Fiehn, O., and Olson, D.E. (2019). Chronic, Intermittent Microdoses of the Psychedelic *N,N*-Dimethyltryptamine (DMT) Produce Positive Effects on Mood and Anxiety in Rodents. ACS Chem. Neurosci. *10*, 3261–3270.

Cameron, L.P., Tombari, R.J., Lu, J., Pell, A.J., Hurley, Z.Q., Ehinger, Y., Vargas, M.V., McCarroll, M.N., Taylor, J.C., Myers-Turnbull, D., et al. (2021). A non-hallucinogenic psychedelic analogue with therapeutic potential. Nature *589*, 474–479.

Chen, T.W., Wardill, T.J., Sun, Y., Pulver, S.R., Renninger, S.L., Baohan, A., Schreiter, E.R., Kerr, R.A., Orger, M.B., Jayaraman, V., et al. (2013). Ultrasensitive fluorescent proteins for imaging neuronal activity. Nature *499*, 295–300.

Chi, T., and Gold, J.A. (2020). A review of emerging therapeutic potential of psychedelic drugs in the treatment of psychiatric illnesses. J. Neurol. Sci. *411*, 116715.

Cussac, D., Boutet-Robinet, E., Ailhaud, M.C., Newman-Tancredi, A., Martel, J.C., Danty, N., and Rauly-Lestienne, I. (2008). Agonist-directed trafficking of signalling at serotonin 5-HT2A, 5-HT2B and 5-HT2C-VSV receptors mediated Gq/11 activation and calcium mobilisation in CHO cells. Eur. J. Pharmacol. *594*, 32–38.

Dunlap, L.E., Andrews, A.M., and Olson, D.E. (2018). Dark Classics in Chemical Neuroscience: 3,4-Methylenedioxymethamphetamine. ACS Chem. Neurosci. *9*, 2408–2427.

Dunlap, L.E., Azinfar, A., Ly, C., Cameron, L.P., Viswanathan, J., Tombari, R.J., Myers-Turnbull, D., Taylor, J.C., Grodzki, A.C., Lein, P.J., et al. (2020). Identification of Psychoplastogenic *N,N*-Dimethylaminoisotryptamine (isoDMT) Analogues through Structure-Activity Relationship Studies. J. Med. Chem. *63*, 1142–1155.

Ebersole, B.J., Visiers, I., Weinstein, H., and Sealfon, S.C. (2003). Molecular basis of partial agonism: orientation of indoleamine ligands in the binding pocket of the human serotonin 5-HT2A receptor determines relative efficacy. Mol. Pharmacol. *63*, 36–43.

Fribourg, M., Moreno, J.L., Holloway, T., Provasi, D., Baki, L., Mahajan, R., Park, G., Adney, S.K., Hatcher, C., Eltit, J.M., et al. (2011). Decoding the signaling of a GPCR heteromeric complex reveals a unifying mechanism of action of antipsychotic drugs. Cell *147*, 1011–1023.

Fukui, M., Rodriguiz, R.M., Zhou, J., Jiang, S.X., Phillips, L.E., Caron, M.G., and Wetsel, W.C. (2007). Vmat2 heterozygous mutant mice display a depressive-like phenotype. J. Neurosci. *27*, 10520–10529.

Glennon, R.A., Young, R., Jacyno, J.M., Slusher, M., and Rosecrans, J.A. (1983). DOM-stimulus generalization to LSD and other hallucinogenic indolealkylamines. Eur. J. Pharmacol. *86*, 453–459.

González-Maeso, J., Yuen, T., Ebersole, B.J., Wurmbach, E., Lira, A., Zhou, M., Weisstaub, N., Hen, R., Gingrich, J.A., and Sealfon, S.C. (2003). Transcriptome fingerprints distinguish hallucinogenic and nonhallucinogenic 5-hydroxytryptamine 2A receptor agonist effects in mouse somatosensory cortex. J. Neurosci. *23*, 8836–8843.

González-Maeso, J., Weisstaub, N.V., Zhou, M., Chan, P., Ivic, L., Ang, R., Lira, A., Bradley-Moore, M., Ge, Y., Zhou, Q., et al. (2007). Hallucinogens recruit specific cortical 5-HT(2A) receptor-mediated signaling pathways to affect behavior. Neuron *53*, 439–452.

González-Maeso, J., Ang, R.L., Yuen, T., Chan, P., Weisstaub, N.V., López-Giménez, J.F., Zhou, M., Okawa, Y., Callado, L.F., Milligan, G., et al. (2008). Identification of a serotonin/glutamate receptor complex implicated in psychosis. Nature *452*, 93–97.

Halberstadt, A.L., Chatha, M., Klein, A.K., Wallach, J., and Brandt, S.D. (2020). Correlation between the potency of hallucinogens in the mouse head-twitch response assay and their behavioral and subjective effects in other species. Neuropharmacology *167*, 107933.

Hanks, J.B., and González-Maeso, J. (2013). Animal models of serotonergic psychedelics. ACS Chem. Neurosci. *4*, 33–42.

Hascoët, M., and Bourin, M. (2009). The Forced Swimming Test in Mice: A Suitable Model to Study Antidepressants. Mood and Anxiety Related Phenotypes in Mice (Springer), pp. 85–118.

Hauser, A.S., Attwood, M.M., Rask-Andersen, M., Schiöth, H.B., and Gloriam, D.E. (2017). Trends in GPCR drug discovery: new agents, targets and indications. Nat. Rev. Drug Discov. *16*, 829–842.

Hilger, D., Masureel, M., and Kobilka, B.K. (2018). Structure and dynamics of GPCR signaling complexes. Nat. Struct. Mol. Biol. *25*, 4–12.

Huot, P., Johnston, T.H., Lewis, K.D., Koprich, J.B., Reyes, M.G., Fox, S.H., Piggott, M.J., and Brotchie, J.M. (2011). Characterization of 3,4-methylenedioxymethamphetamine (MDMA) enantiomers in vitro and in the MPTP-lesioned primate: R-MDMA reduces severity of dyskinesia, whereas S-MDMA extends duration of ON-time. J. Neurosci. *31*, 7190–7198.

Irannejad, R., Tomshine, J.C., Tomshine, J.R., Chevalier, M., Mahoney, J.P., Steyaert, J., Rasmussen, S.G., Sunahara, R.K., El-Samad, H., Huang, B., and von Zastrow, M. (2013). Conformational biosensors reveal GPCR signalling from endosomes. Nature *495*, 534–538.

Kalir, A., and Szara, S. (1963). Synthesis and Pharmacological Activity of Fluorinated Tryptamine Derivatives. J. Med. Chem. *6*, 716–719.

Kenakin, T., and Miller, L.J. (2010). Seven transmembrane receptors as shape-shifting proteins: the impact of allosteric modulation and functional selectivity on new drug discovery. Pharmacol. Rev. *62*, 265–304.

Kim, K., Che, T., Panova, O., DiBerto, J.F., Lyu, J., Krumm, B.E., Wacker, D., Robertson, M.J., Seven, A.B., Nichols, D.E., et al. (2020). Structure of a Hallucinogen-Activated Gq-Coupled 5-HT2A Serotonin Receptor. Cell *182*, 1574–1588.

Ko, K.W., Rasband, M.N., Meseguer, V., Kramer, R.H., and Golding, N.L. (2016). Serotonin modulates spike probability in the axon initial segment through HCN channels. Nat. Neurosci. *19*, 826–834.

Kwon, H.B., Kozorovitskiy, Y., Oh, W.J., Peixoto, R.T., Akhtar, N., Saulnier, J.L., Gu, C., and Sabatini, B.L. (2012). Neuroligin-1-dependent competition regulates cortical synaptogenesis and synapse number. Nat. Neurosci. *15*, 1667–1674.

Li, N., Lee, B., Liu, R.J., Banasr, M., Dwyer, J.M., Iwata, M., Li, X.Y., Aghajanian, G., and Duman, R.S. (2010). mTOR-dependent synapse formation underlies the rapid antidepressant effects of NMDA antagonists. Science *329*, 959–964.

Ly, C., Greb, A.C., Cameron, L.P., Wong, J.M., Barragan, E.V., Wilson, P.C., Burbach, K.F., Soltanzadeh Zarandi, S., Sood, A., Paddy, M.R., et al. (2018). Psychedelics Promote Structural and Functional Neural Plasticity. Cell Rep. *23*, 3170–3182.

Marzaro, G., Guiotto, A., and Chilin, A. (2009). Microwave-promoted mono-N-alkylation of aromatic amines in water: A new efficient and green method for an old and problematic reaction. Green Chem. *11*, 774–776.

Nenajdenko, V.G., Karpov, A.S., and Balenkova, E.S. (2001). A new convenient approach to chiral β-aryl(heteroaryl)alkylamines. Tetrahedron Asymmetry *12*, 2517–2527.

Oh, W.C., Lutzu, S., Castillo, P.E., and Kwon, H.-B. (2016). De novo synaptogenesis induced by GABA in the developing mouse cortex. Science *353*, 1037–1040.

Olsen, R.H.J., DiBerto, J.F., English, J.G., Glaudin, A.M., Krumm, B.E., Slocum, S.T., Che, T., Gavin, A.C., McCorvy, J.D., Roth, B.L., and Strachan, R.T. (2020). TRUPATH, an open-source biosensor platform for interrogating the GPCR transducerome. Nat. Chem. Biol. *16*, 841–849.

Olson, D.E. (2018). Psychoplastogens: A Promising Class of Plasticity-Promoting Neurotherapeutics. J. Exp. Neurosci. *12*, 1179069518800508.

Olson, D.E. (2020). The Subjective Effects of Psychedelics May Not Be Necessary for Their Enduring Therapeutic Effects. ACS Pharmacol. Transl. Sci. Published online December 10, 2020. https://doi.org/10.1021/acsptsci.0c00192.

Patriarchi, T., Cho, J.R., Merten, K., Howe, M.W., Marley, A., Xiong, W.H., Folk, R.W., Broussard, G.J., Liang, R., Jang, M.J., et al. (2018). Ultrafast neuronal imaging of dopamine dynamics with designed genetically encoded sensors. Science *360*, eaat4422.

Preller, K.H., Burt, J.B., Ji, J.L., Schleifer, C.H., Adkinson, B.D., Stämpfli, P., Seifritz, E., Repovs, G., Krystal, J.H., Murray, J.D., et al. (2018). Changes in global and thalamic brain connectivity in LSD-induced altered states of consciousness are attributable to the 5-HT2A receptor. eLife 7, e35082.

Quan, J., and Tian, J. (2011). Circular polymerase extension cloning for high-throughput cloning of complex and combinatorial DNA libraries. Nat. Protoc. 6, 242–251.

Rabin, R.A., Regina, M., Doat, M., and Winter, J.C. (2002). 5-HT2A receptor-stimulated phosphoinositide hydrolysis in the stimulus effects of hallucinogens. Pharmacol. Biochem. Behav. 72, 29–37.

Ren, J., Friedmann, D., Xiong, J., Liu, C.D., Ferguson, B.R., Weerakkody, T., DeLoach, K.E., Ran, C., Pun, A., Sun, Y., et al. (2018). Anatomically Defined and Functionally Distinct Dorsal Raphe Serotonin Sub-systems. Cell 175, 472–487.e20.

Roth, B.L., Irwin, J.J., and Shoichet, B.K. (2017). Discovery of new GPCR ligands to illuminate new biology. Nat. Chem. Biol. 13, 1143–1151.

Schmid, C.L., and Bohn, L.M. (2010). Serotonin, but not N-methyltryptamines, activates the serotonin 2A receptor via a ß-arrestin2/Src/Akt signaling complex in vivo. J. Neurosci. 30, 13513–13524.

Schmid, C.L., Raehal, K.M., and Bohn, L.M. (2008). Agonist-directed signaling of the serotonin 2A receptor depends on beta-arrestin-2 interactions in vivo. Proc. Natl. Acad. Sci. USA 105, 1079–1084.

Shonberg, J., Lopez, L., Scammells, P.J., Christopoulos, A., Capuano, B., and Lane, J.R. (2014). Biased agonism at G protein-coupled receptors: the promise and the challenges–a medicinal chemistry perspective. Med. Res. Rev. 34, 1286–1330.

Somei, M., Yamada, F., Kurauchi, T., Nagahama, Y., Hasegawa, M., Yamada, K., Teranishi, S., Sato, H., and Kaneko, C. (2001). The chemistry of indoles. CIII. Simple syntheses of serotonin, N-methylserotonin, bufotenine, 5-methoxy-N-methyltryptamine, bufobutanoic acid, N-(indol-3-yl)methyl-5-methoxy-N-methyltryptamine, and lespedamine based on 1-hydroxyindole chemistry. Chem. Pharm. Bull. (Tokyo) 49, 87–96.

Stockklausner, C., Ludwig, J., Ruppersberg, J.P., and Klöcker, N. (2001). A sequence motif responsible for ER export and surface expression of Kir2.0 inward rectifier K(+) channels. FEBS Lett. 493, 129–133.

Stoppini, L., Buchs, P.A., and Muller, D. (1991). A simple method for organotypic cultures of nervous tissue. J. Neurosci. Methods 37, 173–182.

Talluri, S.K., and Sudalai, A. (2007). An organo-catalytic approach to the enantioselective synthesis of (R)-selegiline. Tetrahedron 63, 9758–9763.

Tandon, N., Thakkar, K.N., LaGory, E.L., Liu, Y., and Giaccia, A.J. (2018). Generation of Stable Expression Mammalian Cell Lines Using Lentivirus. Bio Protoc. 8, e3073.

Tian, L., Hires, S.A., Mao, T., Huber, D., Chiappe, M.E., Chalasani, S.H., Petreanu, L., Akerboom, J., McKinney, S.A., Schreiter, E.R., et al. (2009). Imaging neural activity in worms, flies and mice with improved GCaMP calcium indicators. Nat. Methods 6, 875–881.

Tombari, R.J., Saunders, C.M., Wu, C.-Y., Dunlap, L.E., Tantillo, D.J., and Olson, D.E. (2019). Ex Vivo Analysis of Tryptophan Metabolism Using 19F NMR. ACS Chem. Biol. 14, 1866–1873.

Unger, E.K., Keller, J.P., Altermatt, M., Liang, R., Matsui, A., Dong, C., Hon, O.J., Yao, Z., Sun, J., Banala, S., et al. (2020). Directed Evolution of a Selective and Sensitive Serotonin Sensor via Machine Learning. Cell 183, 1986–2002.

Wacker, D., Wang, S., McCorvy, J.D., Betz, R.M., Venkatakrishnan, A.J., Levit, A., Lansu, K., Schools, Z.L., Che, T., Nichols, D.E., et al. (2017). Crystal Structure of an LSD-Bound Human Serotonin Receptor. Cell 168, 377–389.e12.

Wan, Q., Okashah, N., Inoue, A., Nehmé, R., Carpenter, B., Tate, C.G., and Lambert, N.A. (2018). Mini G protein probes for active G protein-coupled receptors (GPCRs) in live cells. J. Biol. Chem. 293, 7466–7473.

Wan, J., Peng, W., Li, X., Qian, T., Song, K., Zeng, J., Deng, F., Hao, S., Feng, J., Zhang, P., et al. (2021). A genetically encoded GRAB sensor for measuring serotonin dynamics in vivo. Nat. Neurosci. https://doi.org/10.1038/s41593-021-00823-7.

Yaden, D.B., and Griffiths, R.R. (2020). The Subjective Effects of Psychedelics Are Necessary for Their Enduring Therapeutic Effects. ACS Pharmacol. Transl. Sci. Published online December 10, 2020. https://doi.org/10.1021/acsptsci.0c00194.

Zhang, J.H., Chung, T.D., and Oldenburg, K.R. (1999). A Simple Statistical Parameter for Use in Evaluation and Validation of High Throughput Screening Assays. J. Biomol. Screen. 4, 67–73.

STAR★METHODS

KEY RESOURCES TABLE

REAGENT or RESOURCE	SOURCE	IDENTIFIER
Bacterial and virus strains		
NEB 5-ALPHA COMPETENT E.COLI (HIGH EFFICIENCY) - 6X0.2 ML	NEB	C2987I
rAAV_hSyn_psychLight2	Vigene	N/A
Chemicals, peptides, and recombinant proteins		
lysergic acid diethylamide hemitartrate	NIH Drug Supply Program	N/A
psilocin	NIH Drug Supply Program	N/A
psilocybin	NIH Drug Supply Program	N/A
2-(4-Iodo-2,5-dimethoxyphenyl)ethan-1-amine hydrochloride (2C-I)	NIH Drug Supply Program	N/A
2-bromo-lysergic acid diethylamide tartrate (BOL-148)	NIH Drug Supply Program	N/A
ibogaine hydrochloride	NIH Drug Supply Program	N/A
noribogaine	NIH Drug Supply Program	N/A
cocaine hydrochloride	NIH Drug Supply Program	N/A
salvinorin A	NIH Drug Supply Program	N/A
phencyclidine hydrochloride (PCP)	NIH Drug Supply Program	N/A
serotonin hydrochloride (5-HT)	Fisher	50-120-7920
ketanserin (KETSN)	ApexBio	50-190-5332
ketamine hydrochloride (KET)	Fagron	803647
morphine sulfate	Mallinckrodt	0406-1521-53
lisuride maleate (LIS)	Tocris	40-5210
bromocriptine mesylate	Tocris	04-275-0
(±)-2,5-dimethoxy-4-iodoamphetamine hydrochloride (DOI)	Cayman	13885
imipramine hydrochloride	Cayman	15890
modafinil	Cayman	15417
(±)-threo-methylphenidate hydrochloride	Cayman	11639
indole 3-aceitic acid (3-IAA)	ACROS	AC12216-0250
gramine	ACROS	AC12018-0100
N-acetylserotonin	ACROS	AC22693-1000
melatonin	ACROS	AC12536-2500
tryptamine (TRY)	ACROS	AC15798-0050
N-methyltryptamine (NMT)	ACROS	AC151751000
MDL 100907 (MDL)	Sigma	M3324-5MG
haloperidol	Sigma	H1512
clozapine	Sigma	C6305
aripiprazole	Sigma	SML0935
fluoxetine hydrochloride	Sigma	F132-10MG
rizatriptan benzoate	Sigma	SML0247-10MG
benztropine mesylate	Sigma	SML0847-500MG
(±)-8-hydroxy-2-(dipropylamino)tetralin hydrobromide (8-OH-DPAT)	Sigma	H8520-25MG
R-(-)-apomorphine hydrochloride hemihydrate	Sigma	A4393-100MG
pramipexole hydrochloride	Sigma	PHR1598-500MG
selegiline hydrochloride	Sigma	M003-250MG

Continued

REAGENT or RESOURCE	SOURCE	IDENTIFIER
ladostigil tartrate	Sigma	SML2263-5MG
RuBi-5-HT	Tocris	3856
escitalopram oxalate (ESC)	Tocris	4796
L-glutamic acid (GLU)	Sigma	G1251-500G
g-aminobutyric acid (GABA)	Sigma	A5835-25G
dopamine hydrochloride (DA)	Sigma	H8502-25G
norepinephrine bitartrate (NE)	Sigma	1468501
U50488	Tocris	0495
dimethyl sulfoxide (DMSO)	ACROS	AC327182500
USP grade saline (0.9%)	VWR	68099-103
Tetrodotoxin citrate (TTX)	Tocris	18660-81-6
Sucrose	Sigma-Aldrich	S5016-1KG
HBSS	Fisher	14175103
MgCl	Sigma	M8266-1KG
CaCl$_2$	Sigma	C5670-50G
DMEM	Fisher	11995073
Puromycin	A11138-03	A11138-03
Poly-D-Lysine	Sigma	P6407-5MG
Laminin	Sigma	L2020
dPBS	ThermoFisher	14190-250
Fetal Bovine Serum (FBS)	Fisher	26-140-079
Penicillin-streptomycin	Fisher	15140-163
Carprofen	MWI	24751
Buprenorphine	MWI	O56163
Glutamate	Sigma	G1251
GABA	Sigma	A5835
Dopamine	Sigma	H8502-25G
Norepinephrine	Sigma	74480
Escitalopram	Tocris	4796
Serotonin	Enzo	ALX-550-328-G001
Kanamycin	Fisher	BP906-5
Avertin	Self-made	N/A
2,2,2-Tribromoethanol	Fisher	AC421430500
tert-Amyl Alcohol (Certified)	Fisher	A730-1
2xYT	Self-made	N/A
Tryptone	Fisher	BP1421-500
Yeast Extract	GIBCO	DF0127-17-9
Critical commercial assays		
DNA miniprep kit	QIAGEN	27104
PCR purification kit	QIAGEN	28104
Endo-free Plasmid Maxi kit	QIAGEN	12362
Endo-free Plasmid Maxi kit	QIAGEN	12362
QIAGEN Effectene Transfection kit	QIAGEN	301427
Deposited data		
Raw and analyzed data	This paper	https://github.com/lintianlab/psychLight.
Experimental models: Cells lines		
HEK293T Cells	ATCC	CRL-3216
PSYLI2	This paper	N/A

(*Continued on next page*)

Continued

REAGENT or RESOURCE	SOURCE	IDENTIFIER
Experimental models: Organisms/strains		
E18 Sprague Dawley	Charles River Laboratory	Strain code: 400
C57BL/6J mice	Jackson Laboratory	000664
VMAT2 heterozygous (VMAT2-HET) mice	William C. Wetsel Lab	N/A
Recombinant DNA		
pLVX plasmid with EF1a promotor	Tian Lab	N/A
pCMV_delta8.2	Addgene	12263
pCMV_VSV_G	Addgene	8454
pAAV_hSyn	Addgene	111068
PCMV	Addgene	111054
pCMV_psychLight1	This paper	N/A
pCMV_psychLight2	This paper	N/A
pAAV_hSyn_psychLight2	This paper	N/A
Sequence of psychLight2	This paper	N/A
pCMV_dLight1.1	Tian Lab	N/A
pCMV_dLight1.5	Tian Lab	N/A
pCMV_dLight1.4	Tian Lab	N/A
pCMV_a2AR sensor	Tian Lab	N/A
pCMV_nLight3.1	Tian Lab	N/A
pCMV_kLight1.2a	Tian Lab	N/A
pCMV_GRAB5HT1.0	Subcloned from Addgene	140552
Software and algorithms		
ImageJ	ImageJ	2.0.0-rc-69/1.52p
MATLAB R2019b	Mathworks	RRID:SCR_001622
AnyMaze	Stoelting	6.2
Graphpad Prism 8	Graphpad	8.4.2(464)
SparkControl	Tecan	2.3
Other		
2-photon Microscope	Scientifica	N/A
Vibrating Microtome	Leica	VT1200
Small Animal Stereotax	David Kopf Instruments	1900
Zeiss LSM 710 Confocal	Zeiss	LSM 710
Fluorescent Platereader	Tecan	Spark

RESOURCE AVAILABILITY

Lead contact
Further information and requests for resources and reagents should be directed and will be fulfilled by lead contact, Lin Tian, lintian@ucdavis.edu.

Materials availability
The following plasmids have been deposited in Addgene:

163910	pCMV_psychLight2
163909	pAAV_hSynapsin_psychLight2

AAV Viruses are available through Addgene and the Canadian Neurophotonics Centre.
PSYLI2 cell line will be available upon request via MTA with UCD.

Data and code availability

The full sequence of psychLight has been deposited in GenBank:MW285156 (psychLight1), GeneBank: MW285157 (psychLight2). All source data present in this manuscript are available from https://github.com/lintianlab/psychLight. Custom MATLAB code is available via https://github.com/lintianlab/psychLight.

EXPERIMENTAL MODEL AND SUBJECT DETAILS

Animals

All experimental procedures involving animals were approved by the Institutional Animal Care and Use Committee (IACUC) at the University of California, Davis, the University of Colorado School of Medicine, or Duke University, and adhered to principles described in the National Institutes of Health Guide for the Care and Use of Laboratory Animals. The University of California, Davis, the University of Colorado School of Medicine, and Duke University are accredited by the Association for Assessment and Accreditation of Laboratory Animal Care International (AAALAC).

METHOD DETAILS

Abbreviations (In alphabetical order)

β2AR = beta-2 adrenergic receptor; (S)-Meth-AMPH = (S)-methamphetamine; +Ctrl = positive control; μm = micrometer; 25-CN-NBOH = 4-(2-(2-Hydroxybenzylamino)ethyl)-2,5-dimethoxybenzonitrile hydrochloride; 2C-I = 2-(4-Iodo-2,5-dimethoxyphenyl) ethan-1-amine; 2p = 2-photon; 3-IAA = indole-3-acetic acid; 5-Br-DMT = 5-bromo-N,N-dimethyltryptamine; 5-Cl⁻DMT = 5-chloro-N,N-dimethyltryptamine; 5-F-DMT = 5-flouo-N,N-dimethyltryptamine; 5-HT = serotonin; 5-HT2AR = serotonin 2A receptor; 5-MeO = 5-methoxy-N,N-dimethyltrytamine; 6-F-DET = 6-flouro-N,N-diethyltrytamine; 6-MeO = 6-methoxy-N,N-dimethyltryptamine; 8-OH-DPAT = (±)-8-hydroxy-2-(dipropylamino)tetralin; AAV = adeno-associated virus; AAZ = AAZ-A-154; aCSF = artificial cerebrospinal fluid; BLA = basolateral amygdala; BNST = bed nucleus of the stria terminalis; BOL-148 = 2-bromo- lysergic acid diethylamide; BUFO = bufotenin, N,N-dimethyltryptamine; cpGFP = circularly permuted green fluorescent protein; CPMD = compound; D1R = dopamine receptor D1; DA = dopamine; DMSO = dimethyl sulfoxide; DMT = N,N-dimethyltrytamine; DOI = 2,5-dimethoxy-4-iodoamphetamine; DRN = dorsal raphe nucleus; EC_{50} = half maximal effective concentration; EF1α = human elongation factor-1 alpha; Emax = maximum efficacy; ESC = escitalopram oxalate; FST = forced swim test; GABA = γ-aminobutyric acid; GLU = glutamate; HEK293T = human embryonic kidney 293 cells with SV40 T-antigen; HTR = head-twitch response; IL3 = third intracellular loop; KET = ketamine; KETSN = ketanserin; LIS = lisuride; LSD = lysergic acid diethylamide; LTR = long terminal repeat; MDL = MDL 100907; N-5-HT = N-methylserotonin; N-acetyl-5-HT = N-acetylserotonin; NA = not available; NE = norepinephrine; NMT = N-methyltryptamine; OFC = orbitofrontal cortex; PCP = Phencyclidine; PCP = phencyclidine; PGK = phosphoglycerate kinase; Puro(R) = puromycin resistance; R-AMPH = (R)-amphetamine; R-dimeth-AMPH = (R)-dimethamphetamine; R-MDA = (R)-3,4-methylenedioxyamphetamine; R-MDDMA = (R)-3,4-methylenedioxydimethylamphetamine; R-MDMA = (R)-3,4-methylenedioxy-methamphetamine; ROI = region of interest; S-AMPH = (S)-amphetamine; S-dimeth-AMPH = (S)-dimethamphetamine; S-MDA = (S)-3,4-methylenedioxyamphetamine; S-MDDMA = (S)-3,4-methylenedioxydimethylamphetamine; S-MDMA = (S)-3,4-methylenedioxy-methamphetamine; SEM = standard error mean; STD = standard deviation; TRY = tryptamine; TTX = tetrodotoxin citrate; U50 = U50488; VEH = vehicle; VMAT2-HET = vesicular monoamine transporter 2 heterozygous; W-S = water and 1% sucrose solution; W-W = water and water; WT = wild-type; TBG = Tabernanthalog; ΔF/F = change in fluorescence over initial fluorescence.

Compounds

The NIH Drug Supply Program provided lysergic acid diethylamide hemitartrate, psilocin, psilocybin, 2-(4-Iodo-2,5-dimethoxy-phenyl)ethan-1-amine hydrochloride (2C-I), 2-bromo-lysergic acid diethylamide tartrate (BOL-148), ibogaine hydrochloride, noribogaine, cocaine hydrochloride, salvinorin A, and phencyclidine hydrochloride (PCP). Other chemicals were purchased from commercial sources such as serotonin hydrochloride (5-HT, Fisher, 50-120-7920), ketanserin (KETSN, ApexBio, 50-190-5332), ketamine hydrochloride (KET, Fagron, 803647), morphine sulfate (Mallinckrodt, Inc., 0406-1521-53), lisuride maleate (LIS, Tocris, 40-5210), bromocriptine mesylate (Tocris, 04-275-0), (±)-2,5-dimethoxy-4-iodoamphetamine hydrochloride (DOI, Cayman, 13885), imipramine hydrochloride (Cayman, 15890), modafinil (Cayman, 15417), (±)-threo-methylphenidate hydrochloride (Cayman, 11639), indole 3-aceitic acid (3-IAA, ACROS, AC12216-0250), gramine (ACROS, AC12018-0100), N-acetylserotonin (ACROS, AC22693-1000), melatonin (ACROS, AC12536-2500), tryptamine (TRY, ACROS, AC15798-0050), N-methyltryptamine (NMT, ACROS, AC151751000), MDL 100907 (MDL, Sigma, M3324-5MG), haloperidol (Sigma, H1512), clozapine (Sigma, C6305), aripiprazole (Sigma, SML0935), fluoxetine hydrochloride (Sigma, F132-10MG), rizatriptan benzoate (Sigma, SML0247-10MG), benztropine mesylate (Sigma, SML0847-500MG), (±)-8-hydroxy-2-(dipropylamino)tetralin hydrobromide (8-OH-DPAT, Sigma, H8520-25MG), R-(-)-apomorphine hydrochloride hemihydrate (Sigma, A4393-100MG), pramipexole hydrochloride (Sigma, PHR1598-500MG), selegiline hydrochloride (Sigma, M003-250MG), ladostigil tartrate (Sigma, SML2263-5MG), RuBi-5-HT (Tocris, 3856) escitalopram oxalate (ESC, Tocris, 4796), L-glutamic acid (GLU, Sigma, G1251-500G), γ-aminobutyric acid (GABA, A5835-25G), dopamine hydrochloride (DA, Sigma, H8502-25G), and norepinephrine bitartrate (NE, 1468501). For cellular experiments, the VEH is dimethyl sulfoxide (DMSO, ACROS, AC327182500). For *in vivo* experiments, VEH = USP grade saline (0.9%, VWR, 68099-103). The remaining compounds used in these

studies were synthesized in house and judged to be pure based on NMR and UHPLC-MS. Compounds of the DMT, IsoDMT families (LED-A-4 − LED-C-21) and Tabernanthalog (TBG) were prepared as described previously (Cameron et al., 2021; Dunlap et al., 2020). All enantiopure amphetamines (i.e., amphetamine, methamphetamine, dimethamphetamine) and methylenedioxymethamphetamines (i.e., MDA, MDMA, MDDMA) were prepared using methodology described by Nenajdenko (Huot et al., 2011; Nenajdenko et al., 2001). The key step involved the regioselective ring opening of enantiopure Boc-protected aziridines derived from *R*- and *S*-alaninol, respectively. The Boc-protected amphetamines and methylenedioxymethamphetamines were determined to be enantiomerically pure (> 99 % ee) by chiral HPLC. The methylated amphetamines and methylated methylenedioxyamphetamines were readily prepared using known methods (Dunlap et al., 2020; Talluri and Sudalai, 2007). All amphetamine and methylenedioxyamphetamine derivatives were prepared as the 1:1 fumarate salts with the exception of *R*- and *S*-MDMA, which were prepared as the 2:1 fumarate salts (i.e., hemifumarates). Lastly, *N*-Me-5-HT, *N*-Me-5-MeO-tryptamine hemifumarate, 6-fluorodiethyltryptamine (6-F-DET hemifumarate), 5-bromo-DMT hemifumarate, 5-chloro-DMT hemifumarate, 5-fluoro-DMT hemifumarate, and AAZ-A-137 hemifumarate were prepared using previously reported methods (Blair et al., 2000; Marzaro et al., 2009; Somei et al., 2001; Tombari et al., 2019). Synthetic procedures and characterization data for AAZ-A-154 and LED-C-233 are reported below.

PsychLight Development and Characterization
Development of PsychLight1 and PsychLight2
All constructs were designed using circular polymerase extension cloning (CPEC), restriction cloning, and gBlock gene fragments (Integrated DNA Technologies) (Quan and Tian, 2011). Sequences coding for a FLAG epitope were placed at the 5′ end of the construct as previously described (Irannejad et al., 2013). HindIII and *Not*I cut sites were placed at the 5′- and 3′ ends, respectively, for cloning into pCMV (Addgene) to generate all pCMV constructs. BamHI and HindIII sites were introduced via PCR for final subcloning onto pAAV.hSynapsin1 vectors (Addgene). To maximize coupling between conformational changes and chromophore fluorescence, we chose to use a cpGFP module (LSS-LE-cpGFP-LP-DQL) from GCaMP6 (Chen et al., 2013) for insertion into the human 5-HT2AR using circular polymerase extension cloning (CPEC).

For screening linker variants, we generated linker libraries by first creating an insert DNA carrying a randomized 2 amino acid linker on each side of cpGFP (LSS-xx-cpGFP-xx-DQL). Cloned constructs were amplified and purified with the QIAGEN PCR purification kit prior to NEB® 5-α competent *E. coli* transformation. Competent cells were plated onto kanamycin-containing agar plates. After allowing for 24-hour of growth at 37°C, single colonies were manually picked and grown overnight as described previously (Tian et al., 2009). Plasmids from the colonies were with purified using the QIAGEN miniprep kit. Top variants were sequenced by Genewiz. For conversion of psychLight1 to psychLight2, an ER2 tag was added to the C terminus of the protein, as described previously (Stockklausner et al., 2001), and the two original amino acids from the cpGFP sequence (i.e., F511 and N512, numbering based on psychLight2) were inserted into the N-terminal side of linker 2 to increase the baseline fluorescence. NEB® stable competent cells were transformed with PAAV_hSynapsin_psychLight2. After growth on an agar plate at 30°C, a single colony was selected. After sequencing confirmed the presence of the psychLight2 gene, the cells were expanded at 30°C in 100 mL of growth medium (2xYT), and purified with a QIAGEN Endo-free Plasmid Maxi kit and send to the UC DAVIS Virus Packaging Core for virus production. Sequence information for psychLight1 and psychLight2, see Data S1.

Tissue Culture
HEK293T cells were grown in DMEM, supplemented with fetal bovine serum (FBS) and penicillin-streptomycin. Cells were transfected with Effectene according to the manufacturer's instructions. Prior to imaging, cells were washed with Hank's Balanced Salt Solution (HBSS) supplemented with 2 mM $MgCl_2$ and 2 mM $CaCl_2$. All images were collected in HBSS containing Mg^{2+} and Ca^{2+}.

Transient Transfection of PsychLight1
HEK293T cells were plated and transfected concurrently 24 h prior to each experiment using the QIAGEN Effectene Transfection Reagent kit according to the manufacture's protocol.

Confocal Microscopy Experiments
Dose-response experiments were performed using an Automate Perfusion System. Cells (HEK293T) were grown on 12 mm coverslips and transfected with psychLight1. The coverslips were then placed into a coverslip holder and washed with 5 mL of HBSS containing 2 mM $MgCl_2$ and 2 mM $CaCl_2$. Cells were perfused first with 5 mL of 0.1% DMSO, then drugs in ascending concentrations from 1 pM to 10 µM were added, with the concentration of DMSO being held constant at 0.1%. Images were recorded using a 465 nm laser and a 40x oil objection (0.55 N.A.) on a Zeiss 710 confocal microscope. For the competition studies described in Figure S3, HEK293T cells were prepared as described above; however, the cells were first exposed to 5 mL of 0.2% DMSO. Next, 100 nM 5-HT in 0.2% DMSO was introduced to the cells followed by ascending concentrations of the drug (from 1 pM to 10 µM) in a solution of 100 nM 5-HT, with the concentration of DMSO kept constant at 0.2%. Analysis was performed by taking 3 ROIs on the cell membrane using ImageJ and calculating the mean intensity for each ROI across the time-points. Finally, the ΔF/F was calculated using the average of the baseline (0.1 or 0.2% DMSO) and the average intensity between each dosage over the average of the baseline.

Two-Photon Uncaging Experiments

Organotypic slice cultures from the frontal cortex were prepared from postnatal day 2–3 (P2–P3) C57BL/6J mice, as described previously (Stoppini et al., 1991). Slices were infected 19–20 days prior to imaging by adding a drop of a solution containing 1 μL of concentrated psychLight2 virus (AAV_hSyn_psychLight2) and 4 μL of slice culture media (pre-warmed to 37°C) to the top of the cortical layers. Slices were transfected with tdTomato 17–18 days prior to imaging using biolistic gene transfer (180 psi). Gold particles (6–7 mg) were coated with 12 μg of the tdTomato plasmid (Kwon et al., 2012). Two-photon imaging and uncaging were performed after 21–23 days *in vitro* (DIV) on transfected layer 2/3 pyramidal neurons within 40 μm of the slice surface at 30°C in recirculating artificial cerebrospinal fluid (aCSF; in mM: 127 NaCl, 25 NaHCO$_3$, 1.25 NaH$_2$PO$_4$, 2.5 KCl, 25 D-glucose, aerated with 95% O$_2$/5%CO$_2$) with 2 mM CaCl$_2$, 1 mM MgCl$_2$, 0.1 mM RuBi-5-HT, and 0.001 mM tetrodotoxin. For each neuron, image stacks (512 × 512 pixels; 0.047 μm / pixel) with 1 μm z-steps were collected from one segment of secondary or tertiary apical dendrites 50–80 μm from the soma using a two-photon microscope (Bruker) with a pulsed Ti::sapphire laser (Mai Tai, Spectra Physics) tuned to 920 nm (4–5 mW at the sample). All images shown are maximum projections of 3D image stacks after applying a median filter (2 × 2) to the raw image data. Two-photon uncaging was achieved, as previously described (Oh et al., 2016), except that RuBi-5-HT was used. In brief, the 5-HT uncaging stimulus (1 pulse of 10-ms duration; 17–20 mW at the sample, 810 nm) was delivered by parking the beam at a point ~0.5 μm from the edge of a dendrite with a pulsed Ti::sapphire laser (MaiTai HP, Spectra-Physics). The mock stimulus was identical in parameters to the uncaging stimulus, except carried out in the absence of RuBi-5-HT. Line-scan recording of fluorescence transients was performed simultaneous with 5-HT uncaging on layer 2/3 pyramidal neurons using two pulsed Ti::sapphire lasers for imaging and uncaging at wavelengths of 920 nm and 810 nm, respectively. The fluorescent measurements of psychLight transients were represented as ΔpL2/tdT = [(pL2/tdT) peak / (pL2/tdT) baseline], where pL2 and tdT represent the fluorescence from psychLight2 and tdTomato, respectively. After measuring baseline fluorescences (50 ms), 5-HT uncaging (1 pulse of 10-ms duration, 17–20 mW) was delivered at the target region and peak fluorescences were averaged over 10 ms around the peak. Only cells that showed stable 5-HT-insensitive (Red) signals (< ± 5% fluctuation) were included in our analysis (Oh et al., 2016). To measure changes in psychLight fluorescence intensities following 5-HT bath application (50 μM), fluorescence intensities were calculated from bleed-through-corrected and background subtracted green (psychLight) and red (tdTomato) fluorescence intensities using the integrated pixel intensity of a boxed region surrounding a dendrite and were represented as ΔpL2/tdT = [(pL2/tdT) peak / (pL2/tdT) baseline] (Oh et al., 2016). All statistics were performed across regions of interest (ROIs).

Slice Experiments
Viral Injections

Injection procedures were performed as previously described (Broussard et al., 2018). Briefly, animals were anesthetized using 0.5%–2.5% isoflurane and mounted on a stereotaxic apparatus (Model 900). For injections into the BNST (AP: 0.3 mm, ML: 1 mm, DV: −4.35 mm from the skull), a small craniotomy (1–2 mm diameter) was performed on top of BNST injection site. The virus injection was performed using a Sub-Microliter Injection System with nanofil needles. Three hundred nL of AAV9.*hSynapsin1*.psychLight2 was injected into C57/BL6J mice. Mice were allowed to recover > 2 weeks to allow for sensor expression.

Brain Slices for Two-Photon Imaging

Two to 4 weeks after viral injection, mice were anesthetized with 2.5% avertin and decapitated. The heads were placed into a high-sucrose artificial cerebrospinal fluid (aCSF) solution that contained (in mM): 73 NaCl, 2.5 KCl, 2 MgCl$_2$, 1.25 NaH$_2$PO$_4$, 25 NaHCO$_3$, 24 dextrose, 0.5 CaCl$_2$ and 75 sucrose, saturated with 95% O$_2$ and 5% CO$_2$. The brains were removed from skull and cut (400 μm) with a vibratome (V1200s, Leica) in ice-cold high sucrose aCSF. Brain slices were incubated at 32°C for 30 min before imaging in normal aCSF that contained (in mM): 128 NaCl, 2.5 KCl, 1 MgCl$_2$, 1.25 NaH$_2$PO$_4$, 25 NaHCO$_3$, 10 dextrose and 2 CaCl$_2$, saturated with 95% O$_2$ and 5% CO$_2$. Imaging was carried out at room temperature using a 2-photon microscope. The sensor was excited at 920 nm with a Ti: sapphire laser (Ultra II, Coherent) that was focused by an Olympus 40 × , 0.8NA water immersion objective. Emitted fluorescence was separated by a 525/50 nm filter set, and detected by a photomultiplier (H7422PA-40, Hamamatsu). Data were acquired and collected with ScanImage5 software. Electrical stimulation was performed with a tungsten concentric bipolar microelectrode (TM33CCINS-B, World Precision Instruments).

The area within approximately 20 μm of the electrode was imaged. Rectangular voltage pulses were applied though a 9-channel programmable pulse stimulator (Master-9, A.M.P. Instruments LTD) and a stimulus isolation unit (ISO-Flex, A.M.P. Instruments LTD). Imaging and electrical stimulation were controlled by an Axon Digidata 1550B. Field potentials were applied at 20 pulses with a duration of 0.5 s. Experiments were carried out at a scan rate of 30 (512 × 512 pixels) Hz. Image analysis was performed with ImageJ, data analyses were calculated using MATLAB and SigmaPlot 12.0. Drugs were dissolved as a stock solution in imaging HBSS buffer and diluted at 1:1000 prior to application in the perfusion system.

In vivo PsychLight Recordings
General

At the beginning of surgery, mice were anesthetized with 5% isoflurane for induction and later 1% isoflurane was used for maintenance. After induction of anesthesia, Carprofen (5 mg/kg) and Buprenorphine (1 mg/kg) were subcutaneously injected. The mouse was mounted on a stereotaxic frame. During surgery, body temperature was maintained with a heating pad. Before a sterile scalpel

was used to make an incision, the hair covering the skin above the skull was removed. To have consistent horizontal alignment of the skull, bregma and lambda were leveled to be on the same z axis while two points on the surface of the skull 1.5 mm to either side of lambda were used to level the skull with regard to the y axis. Following viral injection, optical fiber was implanted and secured with metabond and dental cement. Mice were monitored up to 14 days after surgery.

Viral Injection

To inject virus and implant optical fibers for fiber photometry experiments, craniotomy holes were made over the DRN, BNST, BLA, and OFC (DRN, inject with 20° angle, AP: −4.3 mm, ML: 1.1, DV: −2.85 mm; BNST, AP: 0.3 mm, ML: 1 mm, DV: −4.35 mm; BLA, AP: −1.35 mm, ML: 3mm, DV: −4.5 mm; and OFC, AP: 2.5 mm, ML: 1.5 mm, DV: −2.5 mm). Mice were injected with 300 nL of AAV9.*h-Synapsin1*.psychLight2 (BNST, BLA, OFC) or AAV8.*hSynapsin1*.psychLight2 (DRN). Virus was injected using the Sub-Microliter Injection System with nanofil needles. The injection needle was lowered into the brain regions indicated above and infused per site at a rate of 100 nL per min. The injection volume was controlled by a microsyringe pump, which was connected to a controller. Following injection, the virus was allowed to diffuse into the tissue for an additional 10 min before the needle was withdrawn.

Optical Fiber Implantation

After viral injection, optical fibers were mounted into a stereotaxic holder and inserted into tissue targeting 50 μm above the brain regions mentioned above. A layer of Metabond was applied to the surface of the skull around the optical fiber followed by a layer of dental cement to secure the optical fiber.

Auditory Fear Conditioning

Mice were placed into a fear conditioning chamber (Med Associates) with a patch cord connected for photometric recordings. A Doric fiber photometry system was used in this study with 465 nm and 405 nm light (LED, ~30 μW) used for generating the signal and as an isosbestic control, respectively. Each animal received 15 presentations of a 27 s tone (3000 Hz) co-terminating with a foot-shock (0.5 mA for 1.5 s) delivered at 2 min intervals. Each animal received 15 tone/foot-shock pairings over the course of 40 min, and the responses for these trials were averaged to create a single trace per animal. Data analysis was performed with custom-written script in MATLAB. In brief, 405 nm traces were fit with a bi-exponential curve, and then the fit was subtracted from the signal to correct for baseline drift. $\Delta F/F\%$ was calculated as [100*(465 signal - fitted signal) / fitted signal)]. Traces were then z-scored. A heatmap was plotted using a custom MATLAB script by plotting normalized single trials of traces from all animals tested per brain region.

ROC analysis was done by a custom MATLAB script. We first calculated the baseline response from a defined a period of time (fixed measurement time point) before the shock and the sensor response from a defined period of time after the shock from the single trial data. We then calculated the probability distributions for the baseline and response periods by binning the single trial data into two histograms. We then applied a range of thresholds to the two distributions and calculated the true detection rate and false positive rate, which resulted in the ROC curve. Finally, we integrated the area under the ROC curve and approximated the *d'* of the sensor as the discriminability index that had equal area under the ROC curve.

Head-twitch Response with Fiber Photometry

Three animals were used for experiments measuring sensor activity in the prelimbic cortex. A 10 min baseline was recorded prior to compound administration (50 mg/kg 5-MeO or 4 mg/kg KETSN, i.p.) in a 5 mL/kg volume using 0.9% saline as the vehicle. To calculate the $\Delta F/F$ time series, a linear fit was applied to the 405 nm signals and aligned to the 465 nm signals. The fitted 405 nm signal was subtracted from 465 nm channels, and then divided by the fitted 405 nm signal to yield $\Delta F/F$ values. The number of head twitches were counted in 1 min intervals by 2 observers blinded to the treatment conditions and the results were averaged (interpersonnel kappas, Pearson's correlation coefficient = 0.96)

Perfusion and Histology

Stock Avertin was self-made by mixing 10 g of 2,2,2-tribromoethyl alcohol and 10 mL of tert-amyl alcohol. The working stock was diluted to 1.2% (v/v) with water and shielded from light. Animals were euthanized with 125 mg/kg 1.2% Avertin (i.p.) followed by transcardial perfusion with ice-cold 1x phosphate buffered saline (PBS) and subsequently perfused with ice-cold 4% paraformaldehyde (PFA) in 1x PBS. After extraction of the mouse brains, samples were post-fixed in 4% PFA at 4°C overnight. The mouse brains were cryo-protected by immersion in 10% sucrose in a 1x PBS solution overnight. Samples were next placed in 30% sucrose in a 1x PBS solution for > 1 day, before embedding the samples in O.C.T. Samples were then transferred to a −80°C freezer for long-term storage or were sliced into 50 μm sections on a cryostat (Leica Biosystems) for histology. Histology samples were imaged on Zeiss LSM 710 confocal microscope.

High Content Screening with PSYLI2 Cells
Creation of PSYLI2 Cell Line Stably Expressing PsychLight2
The psychLight2 gene was cloned into a pLVX plasmid with the EF1α promotor. The plasmid was transfected into HEK293T cells together with pCMV_delta8.2 and pCMV_VSV_G in a ratio of 10:7:3 using the QIAGEN Effectene Transfection kit. After 14 h of

incubation, the medium was exchanged for fresh DMEM. After an additional 48 h of incubation, the lentivirus-containing medium was collected, filtered through a 0.45 μm Durapore low-protein binding filter, concentrated using a Centricon-70 ultra filtration unit at 3,500 g for 50 min, and stored at −80°C. Next, confluent HEK293T cells that had been grown in 24-well plates were infected with 20 μL of concentrated lentivirus for 48 h. Puromycin selection was performed as described by Tandon and co-workers (Tandon et al., 2018). Expression was assessed via fluorescence microscopy, and a single cell was selected for expansion. The new cell line, named PSYLI2, was frozen in 10% DMSO at −80°C and then transferred to a liquid nitrogen dewar.

High-Content Imaging Experiments
Glass bottom 96-well plates (P96-1.5H-N, Cellvis) were coated with 50 μg/mL of poly-D-lysine (Sigma, P6407-5MG) and 10 μg/mL of laminin (Sigma, L2020) overnight in an incubator (37°C, 5% CO_2). Plates were washed with Dulbecco's PBS (ThermoFisher, 14190-250) and PSYLI2 cells were suspended in DMEM (Fisher, 11995073) containing 10% FBS (Fisher, 26-140-079) with 5% penicillin-streptomycin (Fisher, 15140-163) and plated at a density of 40,000 cells/well 24 h prior to each experiment. Immediately prior to an experiment, stock solutions of drugs in DMSO (10 mM) were diluted 1:100 in imaging media distributed across an empty 96-well plate (treatment plate) in triplicate following a randomized plate map. The imaging media consisted of 1 x HBSS (Fisher, 14175103) containing 0.5 M $MgCl_2$ (Sigma, M8266-1KG) and 0.5 M $CaCl_2$ (Sigma, C5670-50G). Cells grown in a separate 96-well plate (assay plate) were gently washed 3x with imaging media, and the wells were filled with an appropriate volume of imaging media for the respective experiment (*vide infra*).

Agonist Mode
For agonist mode experiments, 180 μL of imaging media were added to each well of the assay plate. Wells were then imaged on a Lecia DMi8 using Leica Application Suite X (V3.6.0.20104) at 40x (N.A. = 0.6) with 5 regions of interest (ROI) taken per well using the default 5 ROI pattern for each well with no bias to location and no overlap of the ROIs (exposure = 350 ms, LED power = 80%). Next, 20 μL from the treatment plate was transferred to the assay plate containing a 1:1000 dilution of drug (10 μM as the final concentration in 0.1% DMSO). As positive, negative, and neutral controls, 5-HT (10 μM), ketanserin (10 μM), and DMSO (0.1%) were used, respectively. All final concentrations of drugs were 10 μM (0.1% DMSO) in agonist mode unless stated otherwise. After 5 min of incubation, the same sites were re-imaged using the same settings.

Once imaging was complete, the images were exported, and analyzed using self-written MATLAB script. Script will be deposit on to Github. In short, segmentation was performed on individual images and a mask highlighting the membrane of the HEK293T cells was generated. Pixel intensities were obtained from the mask-highlighted area and exported into Excel. The ΔF/F values for each well were calculated using the following equation:

$$\frac{(average\ after\ drug - average\ before\ drug)}{average\ before\ drug}$$

These values were then used to obtain the triplicate mean (N = 3).

Antagonist Mode
For antagonist mode experiments, 160 μL of imaging media was added to each well of the assay plate. Wells were imaged on a Lecia DMi8 using Leica Application Suite X (V3.6.0.20104) at 40x (N.A. = 0.6) with 5 regions of interest (ROI) taken per well using the default 5 ROI pattern for each well with no bias to location and no overlap of the ROIs (exposure = 350 ms, LED power = 80%). A 100 μM 5-HT stock solution in DMSO was diluted 1:100 in imaging buffer. Next, 20 μL of this solution was added to the assay plate for a final concentration of 111 nM 5-HT (0.1% DMSO). The same 5 ROIs were imaged after 5 min of incubation. Next, 20 μL from the treatment plate was transferred to the assay plate for a final 1:1000 dilution of drug (10 μM drug, 100 nM 5-HT, 0.2% DMSO). All final concentrations of drugs were 10 μM with 100 nM 5-HT (0.2% DMSO) in antagonist mode unless stated otherwise. After 5 min of incubation, the same sites were re-imaged using the same settings.

Once imaging was complete, the images were exported, and analyzed using self-written MATLAB script. Script will be deposit on to Github. In short, segmentation was performed on individual images and a mask highlighting the membrane of the HEK293T cells was generated. Pixel intensities were obtained from the mask highlighted area and exported into Excel. Then the ΔF/F values for each well were calculated using the following equation:

$$\frac{(average\ after\ drug\&5HT - average\ before\ 5HT)}{average\ before\ 5HT}$$

These values were then used to obtain the triplicate average (N = 3). All imaging and incubation (both agonist and antagonist mode) were performed at ambient atmosphere and temperature.

Calculation of the Ligand Score
Compounds unlikely to bind to the sensor should produce minimal to no response in either agonist or antagonist mode. Therefore, a ligand score was calculated as:

$$\Delta(F/F)_{Compound\ Agonist\ Mode} - \left[(\Delta F/F)_{VEH\ Antagonist\ Mode} - (\Delta F/F)_{Compound\ Antagonist\ Mode}\right]$$

The black heatmap value indicating no effect was set to the value calculated for the vehicle control (i.e., −4.2). The maximal red and blue values were set to those calculated for a prototypical agonist (i.e., LSD, Ligand Score = 21) and antagonist (i.e., MDL100907, Ligand Score = −58), respectively.

Schild Regression Analysis

A treatment plate was prepared by pre-mixing various concentrations of a non-hallucinogenic compound with increasing concentrations of 5-HT. During imaging, 180 μL of imaging media were added to each well of the assay plate. Wells were then imaged on a Lecia DMi8 using Leica Application Suite X (V3.6.0.20104) at 40x (N.A. = 0.6) with 5 regions of interest (ROI) taken per well using the default 5 ROI pattern for each well with no bias to location and no overlap of the ROIs (exposure = 350 ms, LED power = 80%). Next, 20 μL from the treatment plate was transferred to the assay plate for a final 1:1000 dilution of drug. All final drug treatments contained 0.1% DMSO. After 5 min of incubation, the same sites were re-imaged using the same settings. The data analysis method was the same as in agonist and antagonist mode.

Plate reader screening for compound fluorescence

A 96-well plate (UV transparent) was prepared with 100 μL of increasing concentration of BOL-148 and bromocriptine from 10^{-12} to 10^{-5} M together with vehicle control. The plate was read by Tecan Microplate Reader Spark® with excitation wavelength 465 nm (bandwidth 20 nm), emission wavelength 518 nm (bandwidth 20 nm), gain of 120, 5 ROI per well, total 30 flashes per well, and read at z-position 30000 μm from bottom of the plate. All settings controlled by SparkControl software, V2.3.

Antidepressant and Hallucination Related Behavior
Dendritogenesis Experiments

For the dendritogenesis experiments conducted using cultured E18 cortical neurons, timed-pregnant Sprague Dawley rats were obtained from Charles River Laboratories (Wilmington, MA). Full culturing, staining, and analysis details were performed as previously described (Dunlap et al., 2020).

Forced Swim Test (FST)

Male and female C57BL/6J mice (9–10 weeks old at time of experiment, n = 6 of each sex per condition) were obtained from The Jackson Laboratory and housed 4–5 mice of the same sex/cage in a UCD vivarium following an IACUC approved protocol. After 1 week in the vivarium, each mouse was handled for approximately 1 min by a male experimenter for 3 consecutive days prior to the first FST. All experiments were conducted by the same male experimenter who performed the initial handling. During the FST, mice underwent a 6 min swim session in a clear Plexiglas cylinder (40 cm tall, 20 cm in diameter) filled with 30 cm of 24 ± 1°C water. Fresh water was used for every mouse. After handling and habituation to the experimenter, drug-naive mice first underwent a pretest swim to more reliably induce a depressive-like phenotype in subsequent FST sessions. Immobility scores for all mice were determined after the pre-test and mice were assigned to treatment groups to generate groups with similar mean immobility scores used in the following two FST sessions. The next day, the animals received injections (i.p.) of AAZ-A-154 (20 mg/kg), ketamine (3 mg/kg) as the positive control, or vehicle (saline). After 30 min, the animals were subjected to the FST, dried with a towel, and then returned to their home cages. One week later, the FST was performed to assess the sustained effects of the drugs. All FSTs were performed between the hours of 0800 and 1300 h. The experiments were divided into two cohorts either of all males or females and conducted on different days. Experiments were video-recorded and manually scored offline by an experimenter blinded to treatment conditions. Immobility time—defined as passive floating or remaining motionless with no activity other than that needed to keep the mouse's head above water—was scored for the last 4 min of the 6 min trial.

Head-Twitch Response (HTR) and Locomotion Assays

The HTR assay was performed as described previously (Dunlap et al., 2020) using both male and female C57BL/6J mice (2 male and 2 female = 4 total per treatment). The mice were obtained from The Jackson Laboratory (Sacramento, C.A.) and were approximately 8-weeks old at the time of the experiments. Compounds were administered (5 mL/kg, i.p.) using 0.9% saline as the vehicle. After injection, animals were placed into an empty cage (8" x 13" x 5") and HTRs were videotaped, scored later by two blinded observers, and the results were averaged (interpersonnel kappas, Pearson correlation coefficient > 0.91). Locomotion was assessed using AnyMaze automated tracking software.

Sucrose Preference

Adult male and female wild-type (WT) and VMAT2 heterozygous (VMAT2-HET) mice were used for these experiments (Fukui et al., 2007), and they were housed in a humidity- and temperature-controlled room on a 14:10 h light:dark cycle. Mice were housed individually 48 h prior to the experiment with ad libitum access to chow and water. For each day's experiment, bottles were prepared with water or a 1% sucrose solution and these were weighed just prior to the test. Two h prior to the beginning of the dark cycle,

the home-cage water bottle was removed. One h after onset of the dark cycle, a pair of bottles was placed into the home-cage. The mouse was given 2 h to drink, after which the bottles were removed and weighed immediately. Approximately 1 h later, the home-cage water bottle was returned. This procedure was repeated daily with the water-water (W-W) pairing until the mouse showed stable drinking volumes over 3 consecutive days without any side-bias. Once criterion was achieved, the mouse was presented with the water-sucrose (W-S) pairing. The next day (day 1), mice were administered an acute injection of AAZ-A-154 (15 mg/kg, i.p.) and 5 min later were given the W-S pairing (i.e., day 1). Subsequent W-S pairings were presented on days 2 and 4, and then at 4-day intervals. Preference for the sucrose bottle was calculated as the volume of sucrose consumed minus the volume of water consumed, divided by the total volume of liquid consumed. Preference scores approaching "0" indicated no preference for sucrose or water, whereas positive scores signified a preference for sucrose and negative scores denoted a preference for water.

Compound Synthesis
### Synthesis of Previously Uncharacterized Compounds
The syntheses and characterization of most compounds used in this study have been reported previously. Here, we provide synthetic procedures and characterization data (Data S2) for AAZ-A-154 and LED-C-233, as they have not been previously described.

(R)-2-(dimethylamino)propan-1-ol
To an ice-cold solution of R-alaninol (4.93 g, 65.6 mmol) and glacial acetic acid (18.9 mL, 328 mmol, 5.0 equiv) in MeOH (328 mL) was added sodium cyanoborohydride (9.075 g, 144 mmol, 2.2 equiv) followed by 37% formaldehyde$_{(aq)}$ (13.8 mL, 171 mmol, 2.6 equiv). The reaction was stirred at room temperature for 12 h before being concentrated under reduced pressure. The residue was diluted with glycerol (100 mL) and distilled under reduced pressure to yield the pure compound as a colorless oil (6.5 g, 96%), which was used without further purification.
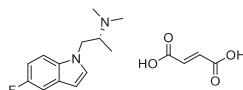
(R)-1-chloro-N,N-dimethylpropan-2-amine hydrochloride
To an ice-cold solution of SOCl$_2$ (2.1 mL, 29 mmol, 1.1 equiv) was added (R)-2-(dimethylamino)propan-1-ol (2.7 g, 26 mmol). The mixture was heated to reflux for 4 h before being concentrated under reduced pressure to yield the desired product as a white solid (3.92 g, 95%), which was used without further purification.
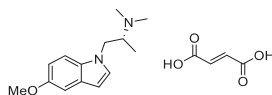
AAZ-A-154
To a solution of 5-methoxyindole (441 mg, 3.00 mmol) in DMSO (7.5 mL) was added (R)-1-chloro-N,N-dimethylpropan-2-amine hydrochloride (664 mg, 4.20 mmol, 1.4 equiv), potassium iodide (697 mg, 4.2 mmol, 1.4 equiv), and potassium tert-butoxide (0943 mg, 8.40 mmol, 2.8 equiv). The reaction mixture was stirred for 24 h, before being diluted with 1.0 M NaOH$_{(aq)}$ (750 mL). The aqueous phase was extracted with DCM (3 × 100mL). The organic extracts were combined, dried over Na$_2$SO$_4$, filtered, and concentrated under reduced pressure to yield a colorless oil, which was purified by flash chromatography (9:1 DCM/MeOH with 1% ammonium hydroxide$_{(aq)}$). The purified oil was dissolved in CHCl$_3$ (3 mL) and added dropwise to a boiling solution of fumaric acid (253 mg, 2.18 mmol, 1.0 equiv) in THF (10 mL). The mixture was concentrated under reduced pressure to yield the desired product as the 1:1 fumarate salt (758 mg, 73%). ^{1}H NMR (600 MHz, DMSO-d_6) δ 7.37 (d, 1H, J = 8.8 Hz), 7.30 (s, 1H), 7.03 (s, 1H, J = 3.1 Hz), 6.76 (d, 1H, J = 8.8 Hz), 6.61 (s, 2H), 6.32 (s, 1H), 4.25 (dd, 1H J = 6.3, 7.8 Hz), 4.02 (dd, 1H, J = 6.3, 7.8 Hz), 3.74 (s, 3H,) 3.11 (q, 1H, J = 6.3, 6.6, Hz), 2.30 (s, 6H), 0.84 (d, 3H, J = 6.6 Hz). ^{13}C NMR (100 MHz, CD$_3$OD) δ 171.0, 155.8, 136.1, 132.8, 130.9, 129.7, 113.3, 111.2, 103.8, 103.3, 61.6, 56.2, 47.5, 39.9, 11.7 ppm.
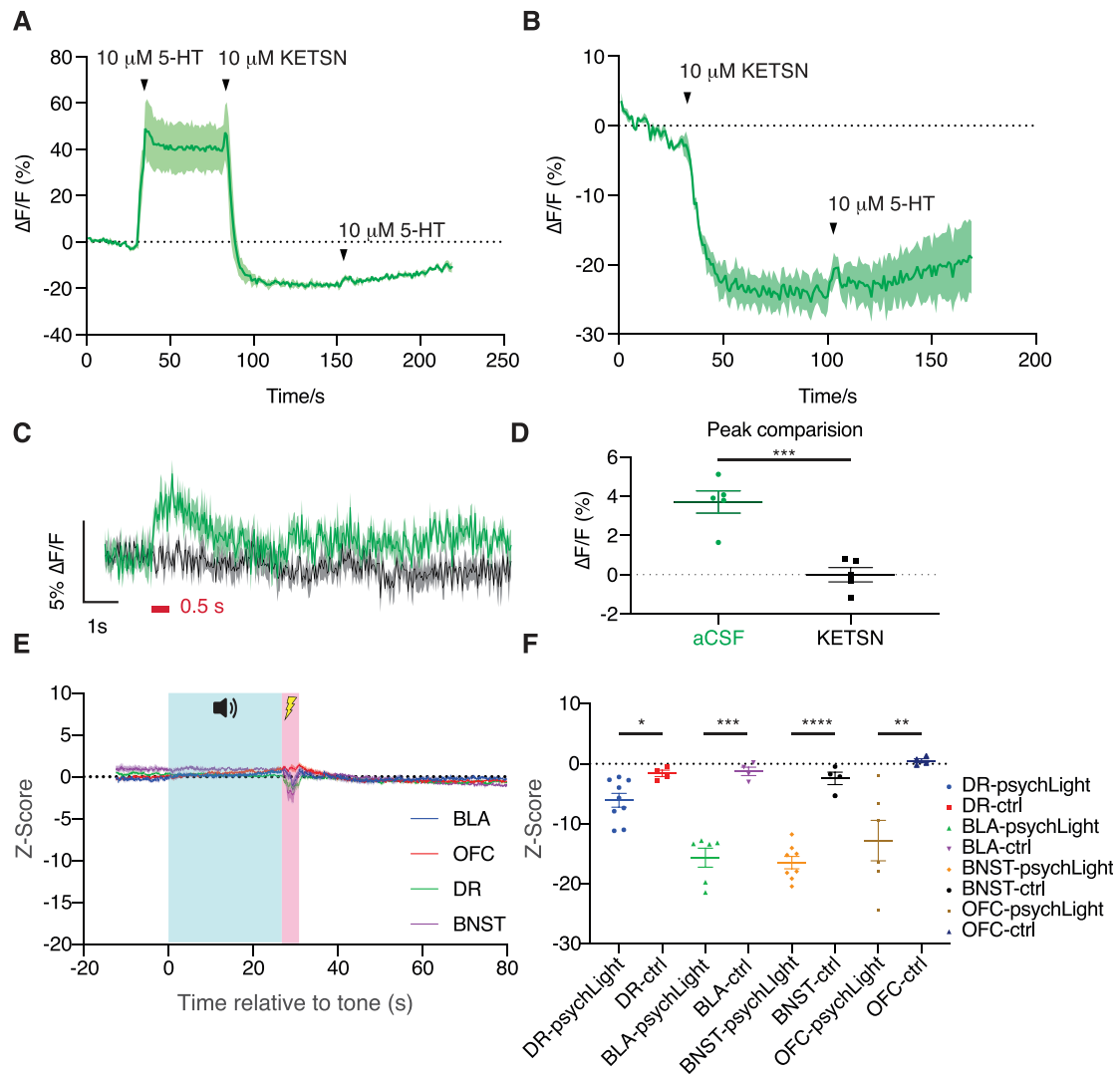

LED-C-233
To a solution of 5-fluoroindole (100 mg, 0.739 mmol) in DMSO (1.90 mL) was added (R)-1-chloro-N,N-dimethylpropan-2-amine hydrochloride (128 mg, 0.814 mmol, 1.1 equiv), potassium iodide (135 mg, 0.814 mmol, 1.1 equiv), and potassium hydroxide (166 mg, 15.8 mmol, 5.0 equiv). The reaction mixture was stirred for 24 h, before being diluted with 1.0 M NaOH$_{(aq)}$ (100mL). The aqueous phase was extracted with DCM (3 × 25 mL). The organic extracts were combined, dried over Na$_2$SO$_4$, filtered, and concentrated under reduced pressure to yield a colorless oil, which was purified by flash chromatography (9:1 DCM/MeOH with 1% ammonium hydroxide$_{(aq)}$). The purified oil was dissolved in acetone (2 mL) and added dropwise to a boiling solution of fumaric acid (48.1 mg, 0.409 mmol, 1.0 equiv) in acetone (5 mL). The mixture was concentrated under reduced pressure to yield the desired product as the 1:1 fumarate salt (111 mg, 54%). ^{1}H NMR (600 MHz, CD$_3$OD) δ 7.49 (m, 1H,), 7.34 (d, 1H, J = 3.2 Hz), 7.25 (dd, 1H, J = 2.5, 9.3 Hz), 6.98 (td, 1H, J = 2.5. 9.3 Hz), 6.72 (s, 2H), 6.53 (d, 1H, J = 3.2 Hz), 4.63 (dd, 1H J = 5.7, 8.9 Hz), 4.35 (dd, 1H, J = 5.7,

8.9 Hz), 3.86 (m, 1H,) 2.84 (s, 6H), 1.21 (d, 3H, J = 6.7 Hz). ^{13}C NMR (100 MHz, CD$_3$OD) δ 171.0, 160.2, 158.7, 136.1, 134.2, 131.1, 130.8, 130.7, 111.5, 111.4, 111.3, 111.1, 106.7, 106.5, 103.6, 103.5, 61.5, 47.6, 40.0, 11.6ppm.

## QUANTIFICATION AND STATISTICAL ANALYSIS

Treatments were randomized, and the data were analyzed by experimenters blinded to the treatment conditions. Statistical analyses were performed using GraphPad Prism (version 8.1.2) unless noted otherwise. All comparisons were planned prior to performing each experiment. The sucrose preference and the volume of liquid consumed in the anhedonia test were analyzed separately by repeated-measures ANOVA using a within subjects' effects of days and a between subjects' effects of genotype with SPSS 27 programs (IBM SPSS Statistics, Chicago, IL). *Post hoc* analyses were by Bonferroni corrected pairwise comparisons. A $p < 0.05$ was considered significant. Data are represented as mean ± SEM, unless otherwise noted, with asterisks indicating *$p < 0.05$, **$p < 0.01$, ***$p < 0.001$, and ****$p < 0.0001$. Details of the statistical tests are displayed in Table S2.

Supplemental figures

Figure S1. Engineering a sensor for hallucinogenic conformations of the 5-HT2A receptor, related to Figure 1

A. Sequence alignment of β2A, DRD1, and 5-HT2A receptors. Initial insertion site of the LSSLI-cpGFP-NHDQL was between K263 and S316 of the 5-HT2AR. The original cpGFP flanking residues (i.e., LI-cpGFP-NH) were chosen based on the sequence of dLight1.3 (Patriarchi et al., 2018). B. After the initial insertion site was determined, a total of 781 variants were screened to optimize psychLight. We screened 766 variants related to the aa composition of the linkers. The top performer (i.e., GY-MH, blue) advanced to the next stage of screening. Next, we performed insertion site optimization of the fluorescent module. A point mutation in TM5 (i.e., E264Q) and removal of 1 aa from TM6 yielded a better variant (red). (TM5 −2aa, TM6 −1aa = −4.2 ± 0.8%. TM5 −1aa, TM6 −1aa = −0.5 ± 0.8%. TM5 +4aa, TM6 −1aa = 10.1 ± 2.2%. Parent (no mutation) = 22.1 ± 3.9%. TM5 +1aa, TM6 −1aa = 37.2 ± 3.2%. TM6 −1aa = 40.8 ± 1.7%. TM5 E264Q, TM6 N317K = 44.2 ± 1.8%. TM5 E264Q, TM6 −1aa = 53.2 ± 0.9%. n = 4 replicates from 4 passages of cells). Next, we made point mutations in intracellular loop 2. The top-performing variant was named psychLight1 (magenta) (P180G/I181G = 33.7 ± 6.8%. P180A/I181A = 34.8 ± 2.5%. Parent (no mutation) = 49.4 ± 5.1%. Q178A/I181A = 49.4 ± 5.1%. I181G = 68.5 ± 1.3%. P180A/I181G = 72.9 ± 5.7%. I181A = 85.2 ± 3.9%). n = 3 replicates from 3 passages of cells. Data are represented as mean ± SEM. ****p < 0.0001, ***p < 0.001, **p < 0.01 and *p < 0.05, one-way ANOVA compares to parent variant within the group with Dunnett's test. C-D. Optimization of psychLight membrane localization. Representative images of HEK293T cells expressing either psychLight1 or psychLight2. Scale bar: 20 μm. Both psychLight1 and psychLight2 are expressed on the cell membranes of HEK293T cells. However, neuronal expression of psychLight1 is primarily intracellular PsychLight2 is expressed on the surface of neurons to a greater extent. AFU = Arbitrary Fluorescence Units.

Figure S2. Control experiments of psychLight recordings in HEK cells ex-vivo and *in vivo*, related to Figures 1 and 2

A–B. Application of 5-HT and KETSN to HEK293T cells in different orders reveals blocking effect of KETSN. A. The order of addition is 10 μM 5-HT followed by 10 μM KETSN and then 10 μM 5-HT. B. The order of addition is 10 μM KETSN followed by 10 μM 5-HT. C. Field stimulation of BNST brain slices followed by two photon imaging of psychLight with either aCSF (green) or a solution of 5-HT2A antagonist KETSN (10 μM, black). The effect of field stimulation was blocked by KETSN. N = 5 slices. D. Quantification of the peak response in C (aCSF: 3.71 ± 0.57%, KETSN: 0 ± 0.36%, ***p < 0.001, unpaired t test). E. Fiber photometry recordings of psychLight0—a control sensor that cannot bind to 5-HT due to a key point mutation (D155A). F. Side by side comparison of psychLight2 and psychLight0 (ctrl) fluorescence during foot shock, indicating psychLight2 is primarily detecting changes in 5-HT concentrations and not simply motion artifacts. DR-psychLight: −6.069 ± 1.165%, DR-ctrl: −1.588 ± 0.5303%, BLA-psychLight: −15.63 ± 1.581%, BLA-ctrl: −1.253 ± 0.7031%, BNST-psychLIght: −16.44 ± 1.034%, BNST ctrl: −2.408 ± 1.033%, OFC-psychLight: −13.79 ± 2.835%, OFC-ctrl: 0.5163 ± 0.3395%, *p < 0.05, **p < 0.01, ***p < 0.001, ****p < 0.0001, unpaired t test compared between each brain region. 5-HT = 5-hydroxytryptamine; KETSN = ketanserin; ctrl = psychLight0; DRN = dorsal raphe nucleus; BNST = bed nucleus of the stria terminalis; BLA = basolateral amygdala; OFC = orbitofrontal cortex.
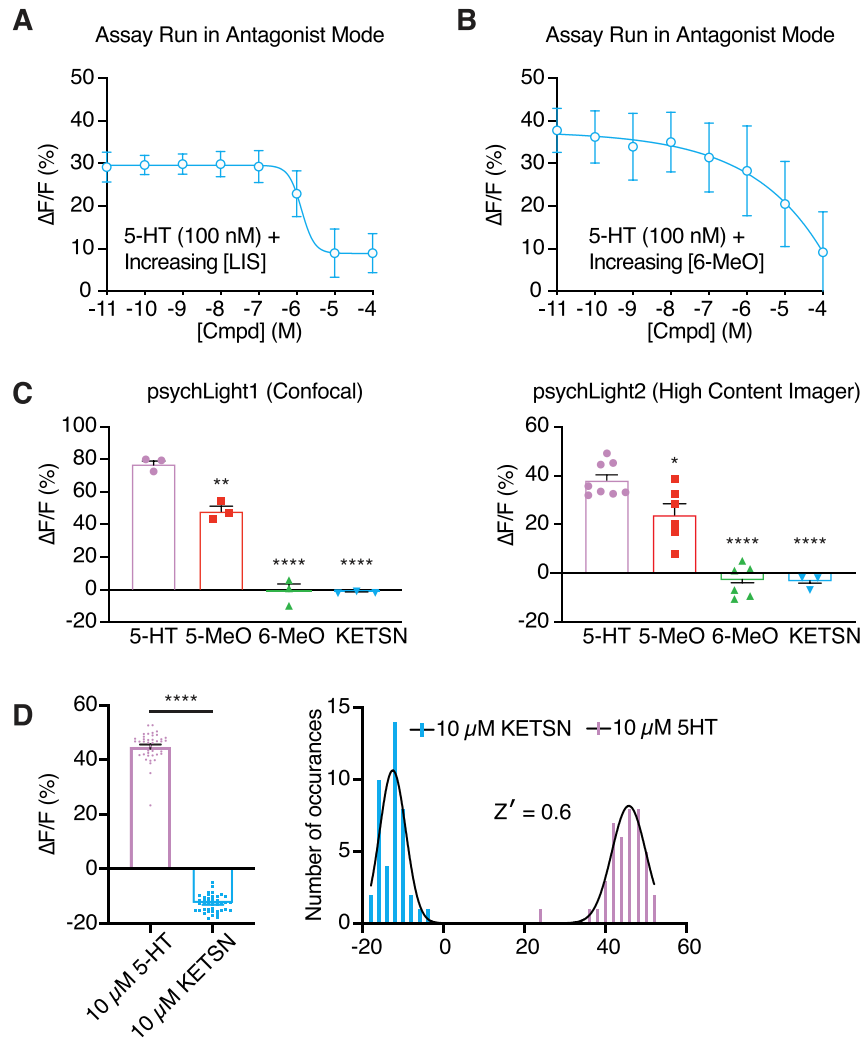
Figure S3. Confocal imaging of psychLight1-expressing HEK293T cells after compound treatments and PSYLI2 characterization, related to Figures 3 and 4

A–B. The non-hallucinogenic ligands lisuride (A) and 6-MeO-DMT (B) can compete off 5-HT resulting in a reduction in psychLight fluorescence. C. PsychLight1 and psychLight2 respond similarly to positive controls (i.e., 5-HT or 5-MeO-DMT at 10 μM) and negative controls (i.e., 6-MeO-DMT or ketanserin at 10 μM). The fluorescence intensities of psychLight1 and psychLight2 were measured using a confocal microscope and a high content imager, respectively (Confocal with psychLight1: $psychLight1_{5\text{-}HT} = 77.3 \pm 2.4\%$, n = 3; $psychLight1_{5\text{-}MeO} = 48.4 \pm 3.1\%$, n = 3; $psychLight1_{6\text{-}MeO} = -1.1 \pm 4.6\%$, n = 3; $psychLight1_{KETSN} = -1.7 \pm 0.3\%$, n = 3. High content imager with psychLight2: $psychLight2_{5\text{-}HT} = 38.2 \pm 2.4\%$, n = 8; $psychLight2_{5\text{-}MeO} = 24.1 \pm 4.6\%$ n = 6; $psychLight2_{6\text{-}MeO} = -3.0 \pm 2.7\%$, n = 6; $psychLight2_{KETSN} = -3.5 \pm 1.6\%$), n = 3. ****$p < 0.0001$, **$p < 0.01$ and *$p < 0.05$, one-way ANOVA compared to 5-HT with Dunnett's test. D. Bar graph showing PSYLI2 response to 10 μM 5-HT (44.8 ± 0.8%) and 10 μM KETSN (−12.7 ± 0.5%), and frequency distribution of both positive (magenta, 5-HT) and negative (blue, KETSN) control treatments (Z-factor$_{PSYLI2}$ = 0.6), n = 42. ****$p < 0.0001$, unpaired t test.
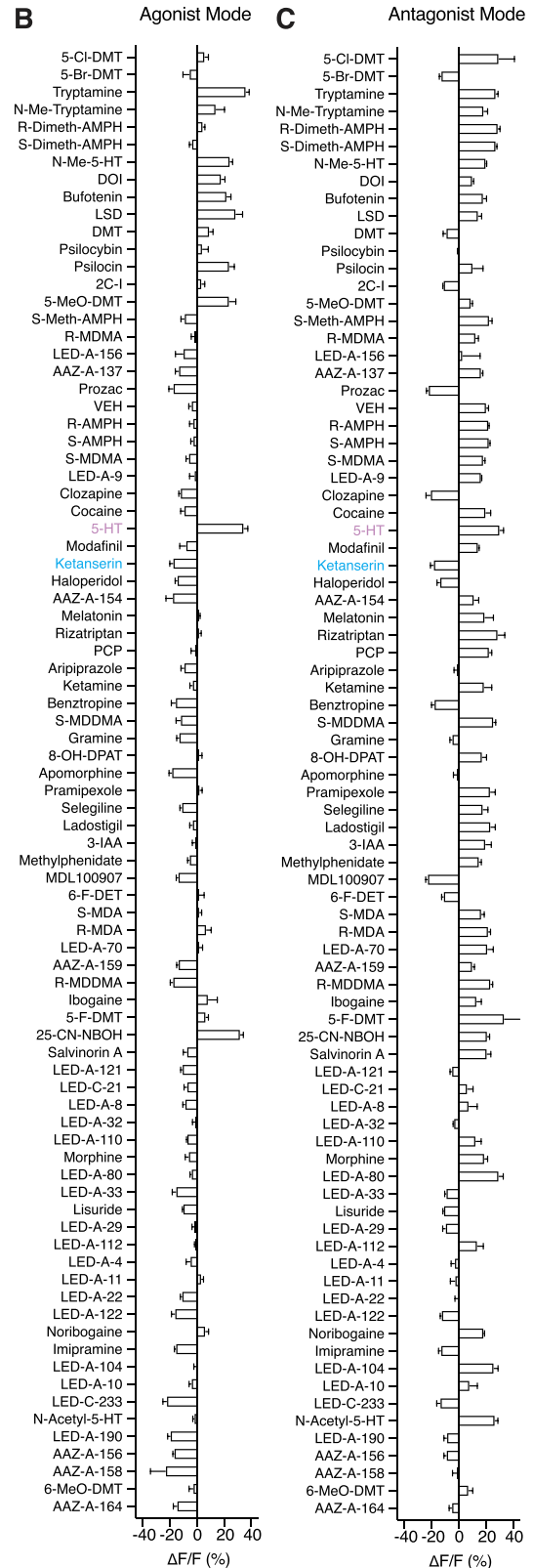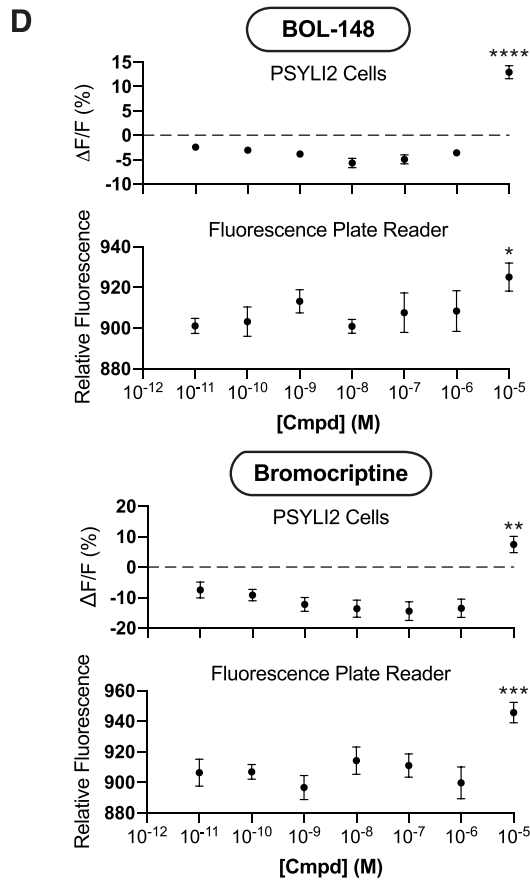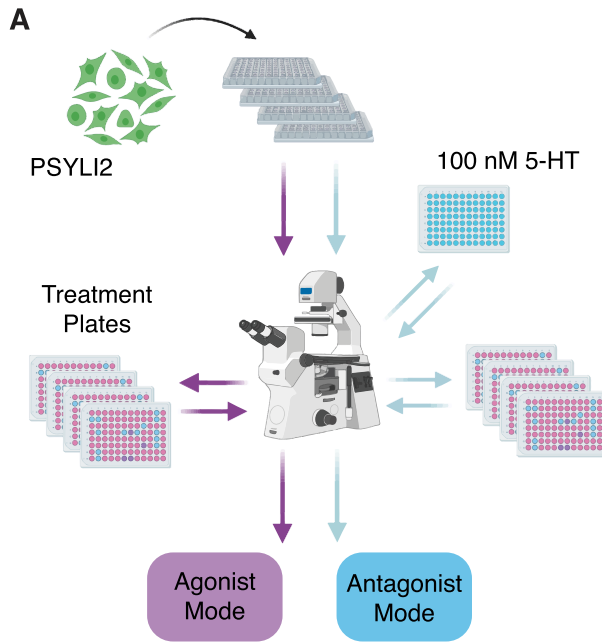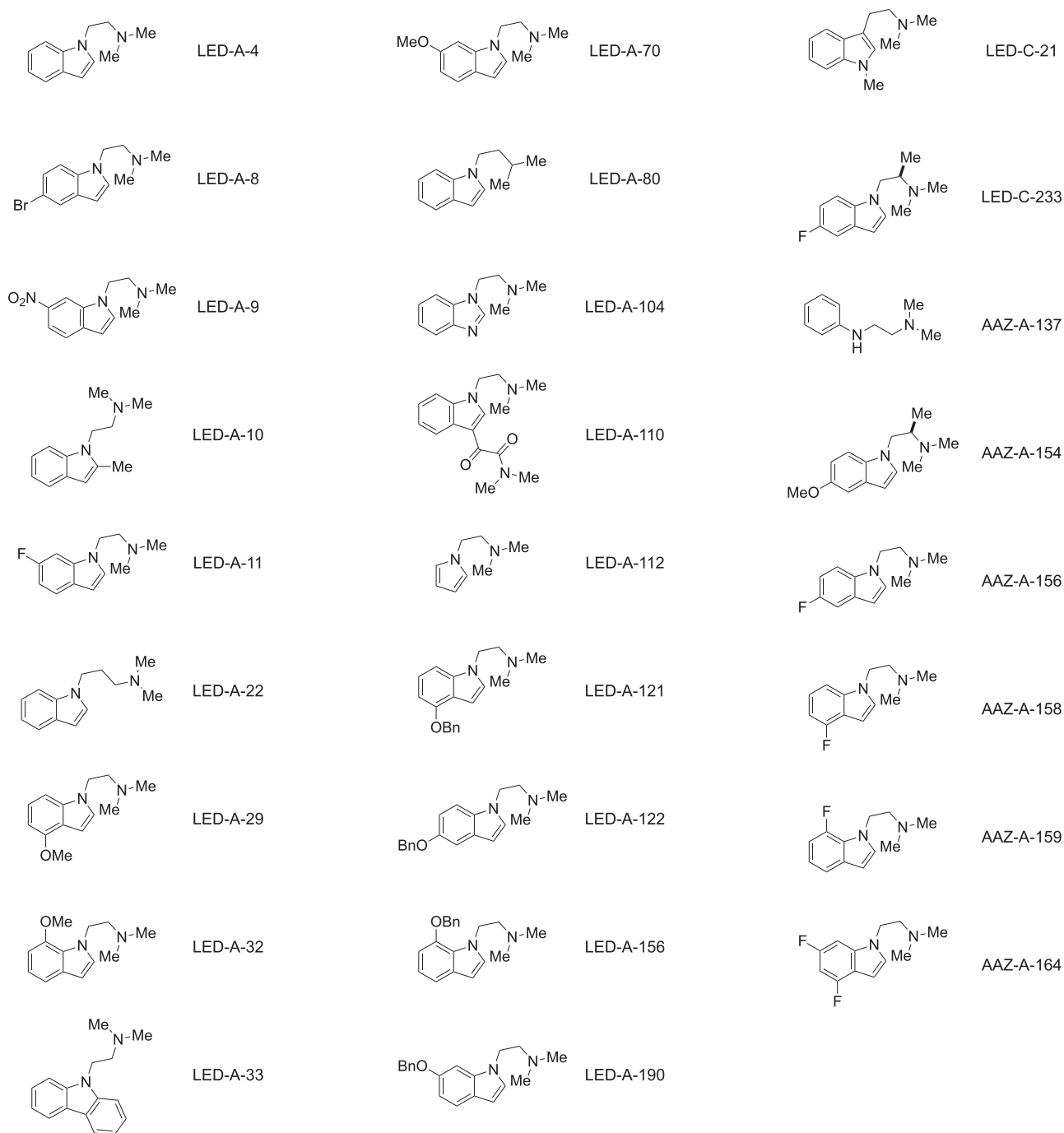
Figure S4. Characterization of PSYLI2 cells and their use in high content screening, related to Figure 4

A. Schematic depicting the workflow for a screening campaign using both agonist and antagonist modes. B. Agonist mode screen of a compound library using PSYLI2 cells. C. Antagonist mode screen of a compound library using PSYLI2 cells. D. Concentration-response studies using PSYL2 cells (top) and a cell free wells (bottom) reveal that BOL-148 and bromocriptine produce fluorescence artifacts at 10 μM (****$p < 0.0001$, ***$p < 0.001$, **$p < 0.01$ and *$p < 0.05$, one-way ANOVA compares to parent variant within the group with Dunnett's test). Data are represented as mean ± SEM 5-HT = 5-hydroxytryptamine; KETSN = ketanserin; BOL-148 = 2-bromolysergic acid diethylamide.

LED-A-4

LED-A-8

LED-A-9

LED-A-10

LED-A-11

LED-A-22

LED-A-29

LED-A-32

LED-A-33

LED-A-70

LED-A-80

LED-A-104

LED-A-110

LED-A-112

LED-A-121

LED-A-122

LED-A-156

LED-A-190

LED-C-21

LED-C-233

AAZ-A-137

AAZ-A-154

AAZ-A-156

AAZ-A-158

AAZ-A-159

AAZ-A-164

Figure S5. Chemical structures of compounds synthesized in house, related to Figure 4
Syntheses and characterization data for compounds are shown in the supporting information.
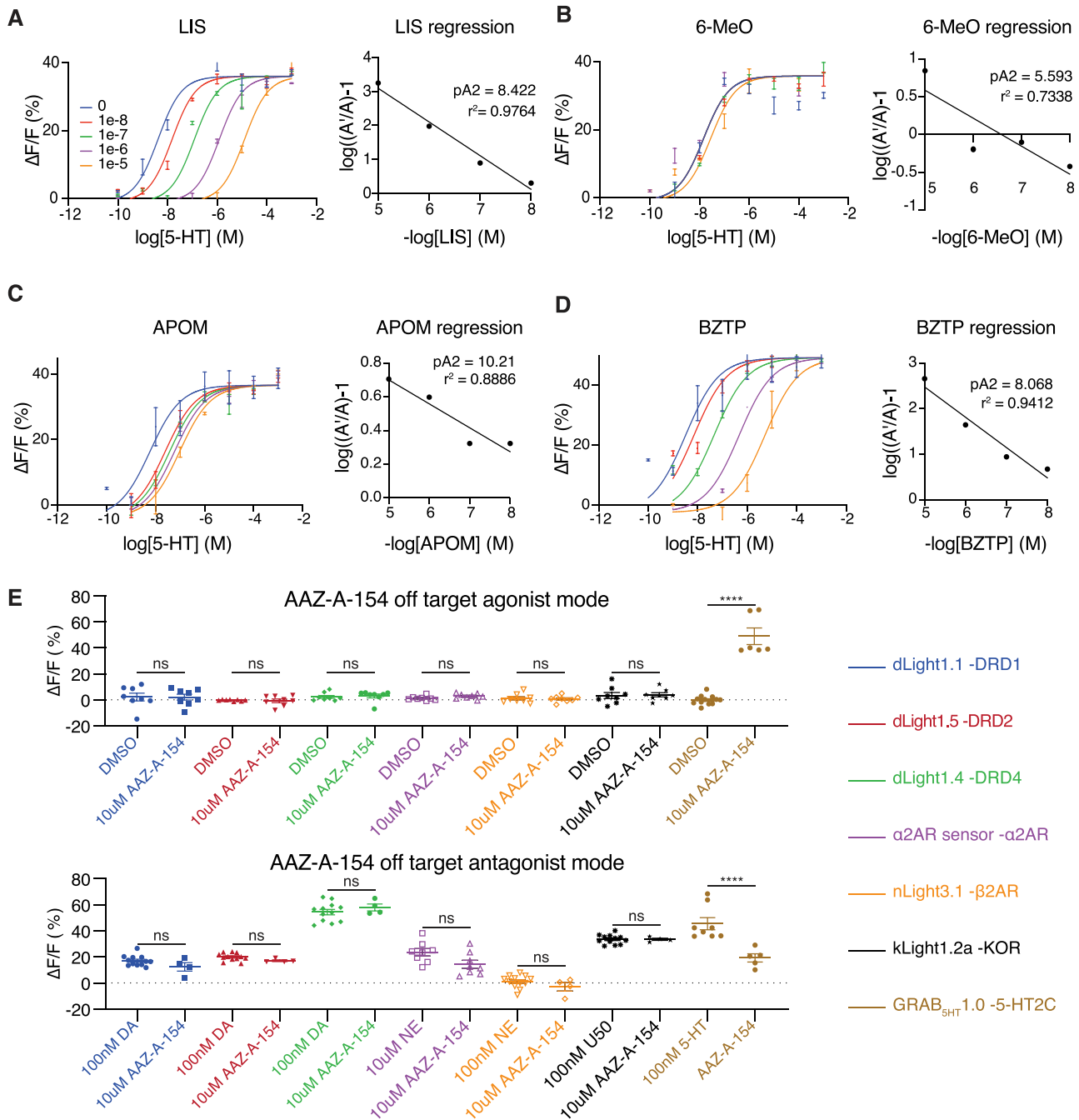
Figure S6. Schild regression analysis for non-hallucinogenic 5-HT2AR ligands and off target characterization for AAZ-A-154, related to Figures 4 and 5

A–D. Schild analysis using 5-HT (100 nM) as the agonist and 4 concentrations of non-hallucinogenic compounds (i.e., LIS, 6-MeO, apomorphine, benztropine). LIS = lisuride, 6-MeO = 6-MeO-DMT, APOM = apomorphine, BZTP = benztropine. E. Data from agonist and antagonist mode of 7 receptor-based sensors (Agonist mode: 0.1% DMSO or 10 μM AAZ-A-154 was added; Antagonist mode: 0.1% DMSO or 10uM AAZ-A-154 was added in the presence of 100 nM dopamine (DA), norepinephrine (NE), U-50488 (U50) or serotonin(5-HT)). ****p < 0.0001, ns p > 0.05. One-way ANOVA. Tukey's multiple comparisons test.

Supplemental information

Psychedelic-inspired drug discovery

using an engineered biosensor

Chunyang Dong, Calvin Ly, Lee E. Dunlap, Maxemiliano V. Vargas, Junqing Sun, In-Wook Hwang, Arya Azinfar, Won Chan Oh, William C. Wetsel, David E. Olson, and Lin Tian

Supplementary Data 1. PsychLight1 and psychLight2 protein sequences. Related to STAR Methods.

psychLight1.prot (695 aa)

```
MKTIIALSYIFCLVFADYKDDDDAMDILCEENTSLSSTTNSLMQLNDDTRLYSND
1|        10|        20|        30|        40|        50|

FNSGEANTSDAFNWTVDSENRTNLSCEGCLSPSCLSLLHLQEKNWSALLTAVVII
   60|        70|        80|        90|       100|       110|

LTIAGNILVIMAVSLEKKLQNATNYFLMSLAIADMLLGFLVMPVSMLTILYGYRW
      120|       130|       140|       150|       160|

PLPSKLCAVWIYLDVLFSTASIMHLCAISLDRYVAIQNPAHHSRFNSRTKAFLKI
   170|       180|       190|       200|       210|       220|

IAVWTISVGISMPIPVFGLQDDSKVFKEGSCLLADDNFVLIGSFVSFFIPLTIMV
      230|       240|       250|       260|       270|

ITYFLTIKSLQKQLSSGYNVYIKADKQKNGIKANFKIRHNIEDGGVQLAYHYQQN
   280|       290|       300|       310|       320|       330|

TPIGDGPVLLPDNHYLSVQSKLSKDPNEKRDHMVLLEFVTAAGITLGMDELYKGG
      340|       350|       360|       370|       380|

TGGSMVSKGEELFTGVVPILVELDGDVNGHKFSVSGEGEGDATYGKLTLKFICTT
   390|       400|       410|       420|       430|       440|

GKLPVPWPTLVTTLTYGVQCFSRYPDHMKQHDFFKSAMPEGYIQERTIFFKDDGN
      450|       460|       470|       480|       490|

YKTRAEVKFEGDTLVNRIELKGIDFKEDGNILGHKLEYNMHDQLNEQKACKVLGI
   500|       510|       520|       530|       540|       550|

VFFLFVVMWCPFFITNIMAVICKESCNEDVIGALLNVFVWIGYLSSAVNPLVYTL
      560|       570|       580|       590|       600|

FNKTYRSAFSRYIQCQYKENKKPLQLILVNTIPALAYKSSQLQMGQKKNSKQDAK
   610|       620|       630|       640|       650|       660|

TTDNDCSMVALGKQHSEEASKDNSDGVNEKVSCV*
      670|       680|       690|      |695
```

```
MKTIIALSYIFCLVFADYKDDDDAMDILCEENTSLSSTTNSLMQLNDDTRLYSND
1|        10|          20|          30|          40|          50|

FNSGEANTSDAFNWTVDSENRTNLSCEGCLSPSCLSLLHLQEKNWSALLTAVVII
   60|          70|          80|          90|         100|         110|

LTIAGNILVIMAVSLEKKLQNATNYFLMSLAIADMLLGFLVMPVSMLTILYGYRW
        120|         130|         140|         150|         160|

PLPSKLCAVWIYLDVLFSTASIMHLCAISLDRYVAIQNPKHHSRFNSRTKAFLKI
   170|         180|         190|         200|         210|         220|

IAVWTISVGISMPIPVFGLQDDSKVFKEGSCLLADDNFVLIGSFVSFFIPLTIMV
        230|         240|         250|         260|         270|

ITYFLTIKSLQKQLSSGYNVYIKADKQKNGIKANFKIRHNIEDGGVQLAYHYQQN
   280|         290|         300|         310|         320|         330|

TPIGDGPVLLPDNHYLSVQSKLSKDPNEKRDHMVLLEFVTAAGITLGMDELYKGG
        340|         350|         360|         370|         380|

TGGSMVSKGEELFTGVVPILVELDGDVNGHKFSVSGEGEGDATYGKLTLKFICTT
   390|         400|         410|         420|         430|         440|

GKLPVPWPTLVTTLTYGVQCFSRYPDHMKQHDFFKSAMPEGYIQERTIFFKDDGN
        450|         460|         470|         480|         490|

YKTRAEVKFEGDTLVNRIELKGIDFKEDGNILGHKLEYNFNMHDQLNEQKACKVL
   500|         510|         520|         530|         540|         550|

GIVFFLFVVMWCPFFITNIMAVICKESCNEDVIGALLNVFVWIGYLSSAVNPLVY
        560|         570|         580|         590|         600|

TLFNKTYRSAFSRYIQCQYKENKKPLQLILVNTIPALAYKSSQLQMGQKKNSKQD
   610|         620|         630|         640|         650|         660|

AKTTDNDCSMVALGKQHSEEASKDNSDGVNEKVSCVFCYENEV*
        670|         680|         690|         700|    |704
```

Supplementary Data 2. Novel compound characterizations. Related to STAR Methods.
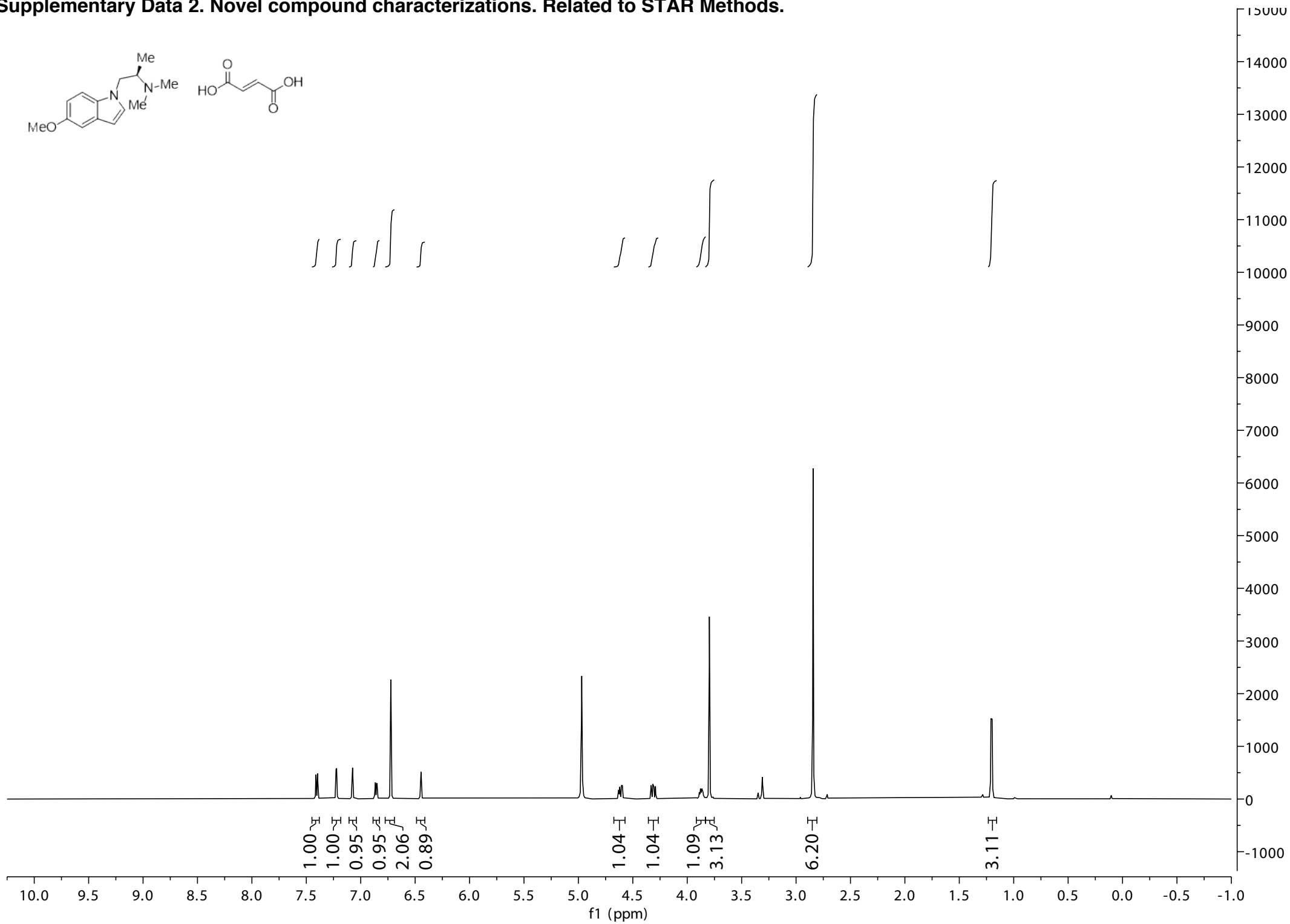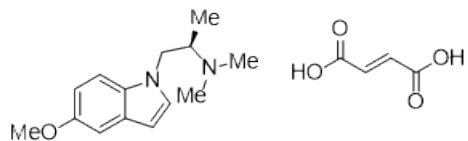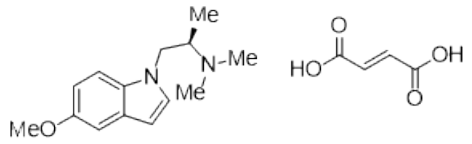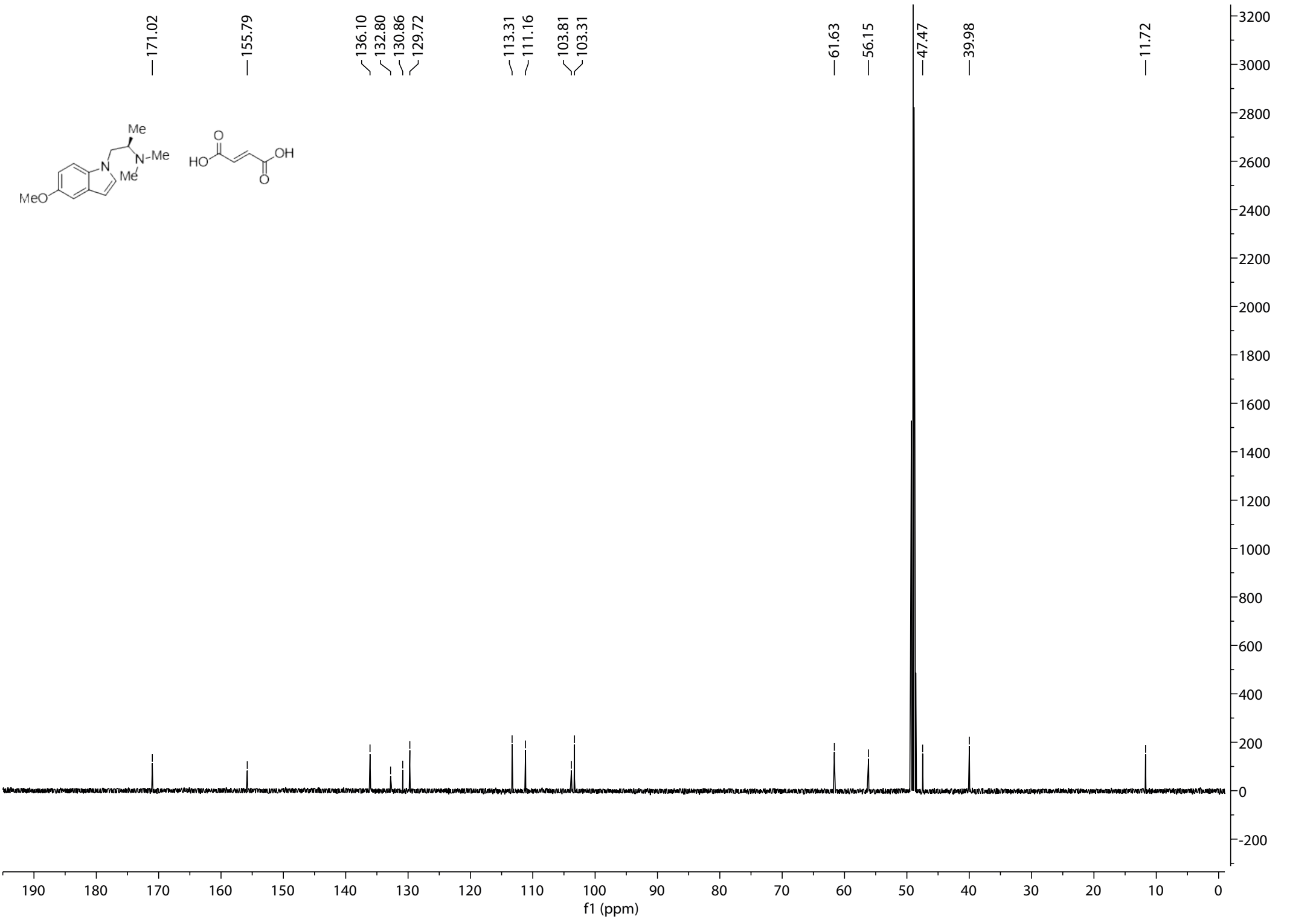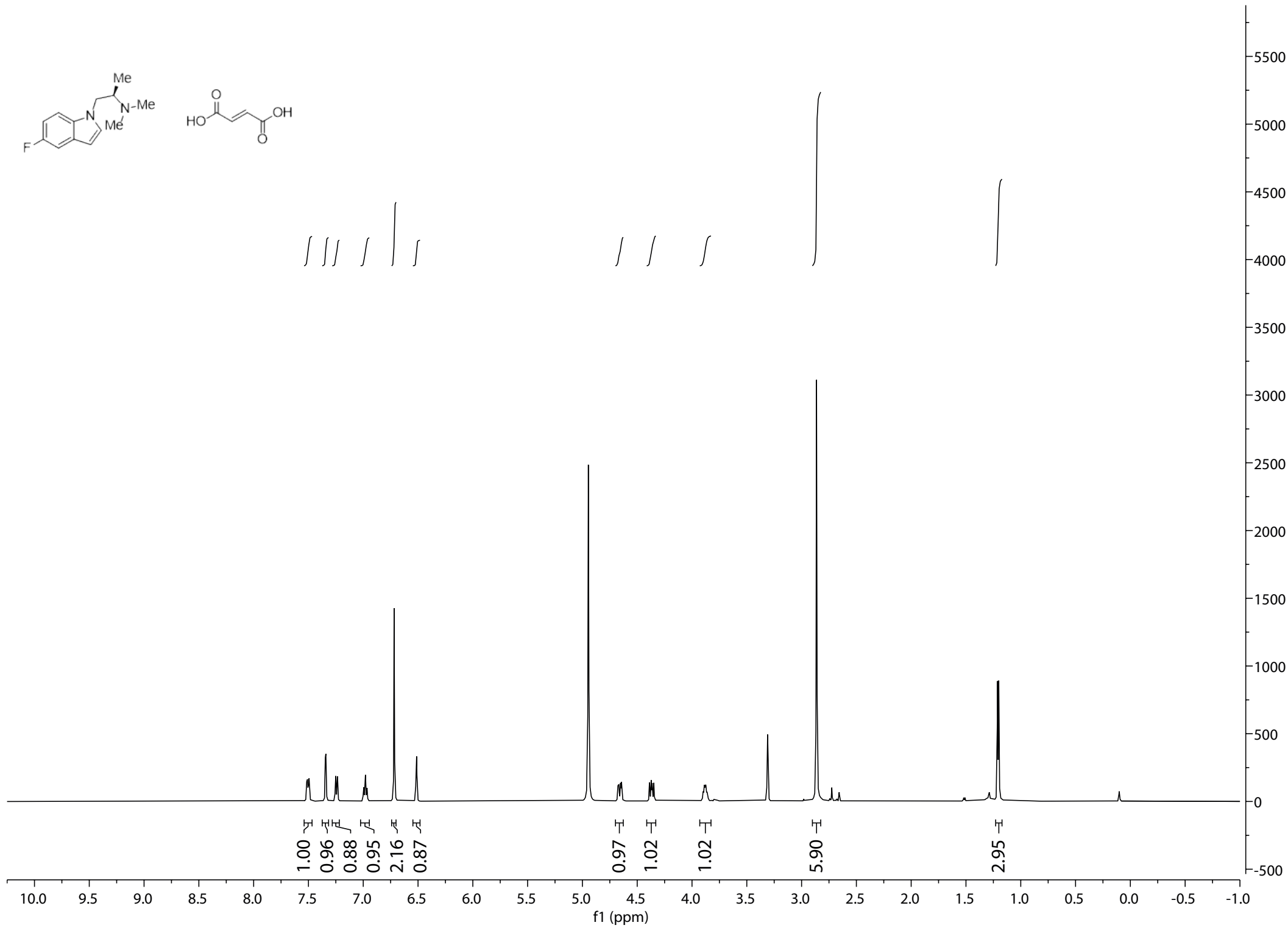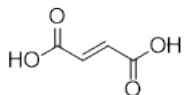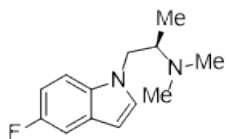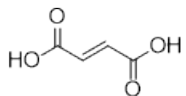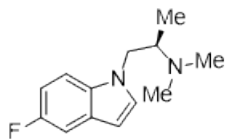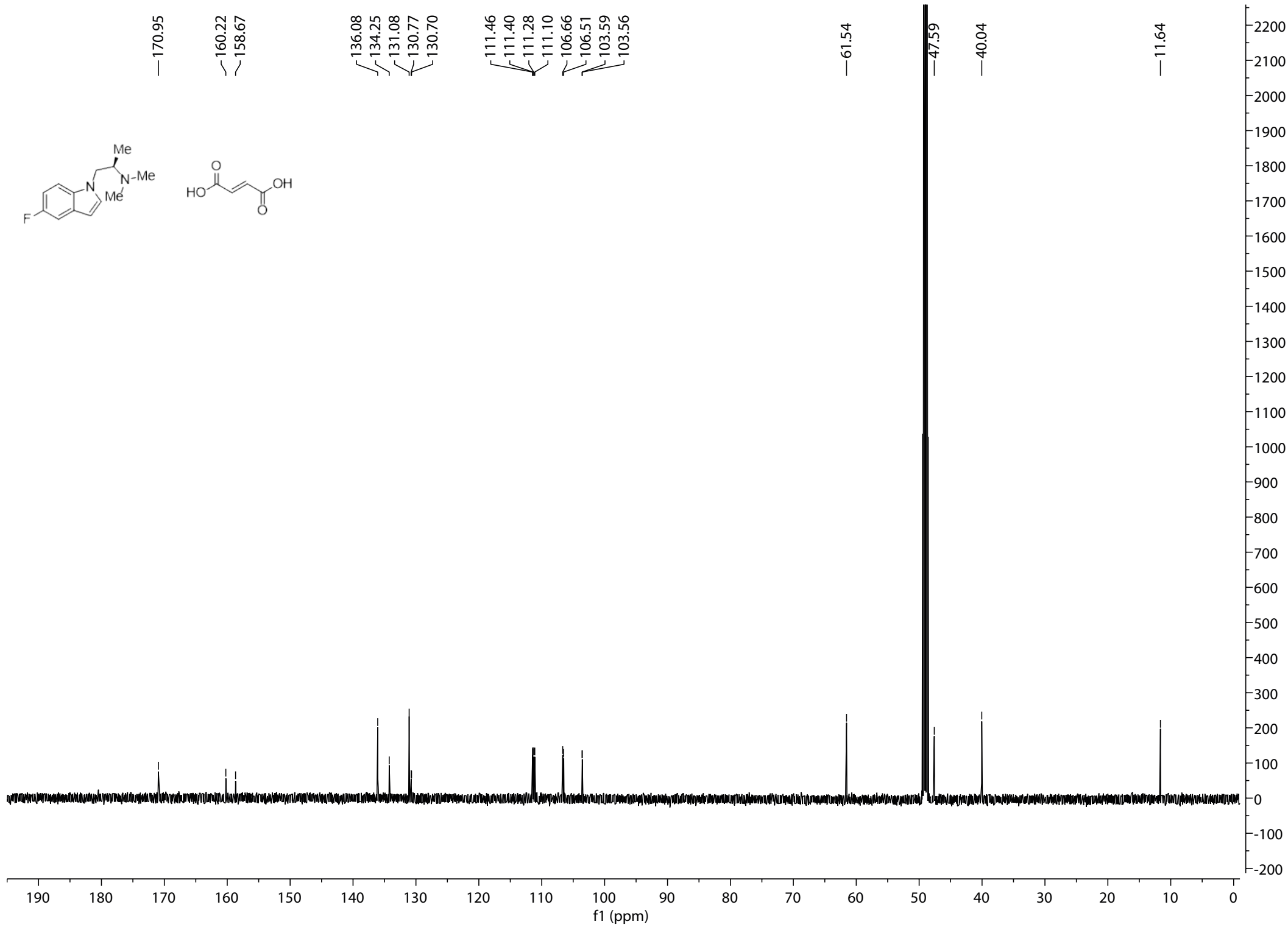
Supplementary Table 1. Overview of experimental design and results. Related to all Figures.

Question	Approach	Results	Figures
Development of psychLight for imaging serotonin and hallucinogens			
Can we design a sensor to probe ligand-induced conformational changes of 5-HT2A receptor?	We replaced the third intracellular loop of the 5-HT2A receptor with cpGFP followed by linker screening and membrane localization optimization	psychLight responded to serotonin, but not to 5-HT2AR antagonists. Serotonin displayed an EC_{50} = 26.3 nM	Figure 1A–D
What is the sensitivity and kinetics of psychLight?	Two-photon uncaging and imaging of serotonin in cultured cortical slices	psychLight displayed fast off kinetics (5.4 ms) in response to single pulse uncaging (10ms)	Figure 1E–H
	Two-photon imaging of serotonin release triggered by electrical stimuli in acute slices	psychLight was able to detect electrically-evoked serotonin release in BNST acute slices. The fluorescence response can be modulated by a SSRI and abolished by a sodium channel blocker TTX and a serotonin receptor antagonist granisetron	Figure 1I–M
In vivo imaging of serotonin release in multiple brain regions with fiber photometry			
Can psychLight detect behaviorally relevant serotonin release?	We applied fiber photometry to study endogenous serotonin release in DRN, BNST, BLA, and OFC triggered by auditory fear conditioning	psychLight can faithfully detect the serotonin dynamics across the full-course of fear-learning in single trials (d'>12).	Figure 2
Imaging hallucinogenic conformations of 5-HT2AR			
Can psychLight be used to detect activation of 5-HT2AR by hallucinogens in vivo?	In vivo fiber-photometry recording in mPFC	Fluorescence increased upon administration of 5-MeO-DMT and the onset of increase correlated with the head-twitch response	Figure 3A–C
How effectively do hallucinogenic compounds activate psychLight?	Concentration-response curve in 293T cells	Determined EC_{50} values for a panel of hallucinogens	Figure 3D–G
		PsychLight EC_{50} values correlate with human hallucinogenic potency	Figure 3H
		PsychLight response is not equivalent to other measures of 5-HT2AR activation	Figure 3I
Medium-throughput pharmacological assay based on psychLight			
Can we use psychLight to establish a cell-based assay for determining hallucinogenic potentials of library compounds?	Engineered HEK293T cell line stably expressing psychLight2	Z-score of the assay is 0.6	Figure S3D
		The assay is sensitive to compounds with similar molecular structures	Figure 4B–C
	Screened a library consisting of hallucinogens, non-halluci-nogens, and a panel of compounds with unknown hallucinogenic potentials	Defined a ligand score to predict the pahrmacological features of compounds: Ligand score >0: 5-HT2AR-activating hallucinogens Ligand score <0: non-hallucinogenic 5-HT2AR ligands Ligand score ~0: not 5HT2AR ligands	Figure 4D–E
		Schild regression analysis defined non-hallucinogenic ligands as competative antagonists	Figure 5D Figure S6
Identification of new hallucinogenic and non-hallucinogenic compounds			
Will predicted hallucinogens produce hallucinogenic behaviors?	Performed a three-point dose-response study of 5-halo-DMT family measuring head-twitch response and locomotion	5-F-DMT and 5-Cl-DMT produce robust HTR as predicted by psychLight 5-Br-DMT did not produce a HTR as predicted by psychLight	Figure 5A–C
What are the pharmacological features and behavioral effects of predicted non-hallucinogens, such as AAZ-A-154 ?	Performed Schild regression analysis Performed a three-point dose-response study measuring head-twitch response and locomotion	AAZ-A-154 is a competitive 5-HT2AR ligand that did not produce a HTR as predicted by psychLight	Figure 5D–F
Characterizing antidepressant-like effects of a novel non-hallucinogenic compound			
Can AAZ-A-154 promote dendritic growth in cultured neurons? If yes, is the effect 5-HT2R dependent?	Performed Sholl analysis in cultured cortical neurons treated with AAZ-A-154 or vehicle in the presence and absence of 5HT2R antagonist ketanserin	AAZ-A-154 promoted dendritic growth. This effect can be blocked by ketanserin, implicating 5-HT2Rs in the mechanism of action	Figure 6A–C
Does AAZ-A-154 have antidepressant potential? If yes, is the effect comparable to Ketamine?	Performed forced swim test	AAZ-A-154 produces both rapid (30 min) and long-lasting (1 week) antidepressant-like effects after a single administration comparable to ketamine	Figure 6D
	Measured anhedonia in a genetic animal model relevant to depression	VMAT2-HET mutants exhibited a sucrose preference that was indistinguishable from WT controls after a single-adminis-tration and the effect was long-lasting (12-days)	Figure 6E